12-2022

Measurement and Evaluation of Roadway Geometry for Safety Analyses and Pavement Material Volume Estimation for Resurfacing and Rehabilitation Using Mobile LiDAR and Imagery-based Point Clouds

Leonildo Nelson Cassule
lcassul@clemson.edu

MEASUREMENT AND EVALUATION OF ROADWAY GEOMETRY FOR SAFETY ANALYSES AND PAVEMENT MATERIAL VOLUME ESTIMATION FOR RESURFACING AND REHABILITATION USING MOBILE LIDAR AND IMAGERY-BASED POINT CLOUDS

A Dissertation
Presented to
the Graduate School of
Clemson University

In Partial Fulfillment
of the Requirements for the Degree
Doctor of Philosophy
Civil Engineering

---

by
Leonildo Nelson Cassule
December 2022

Accepted by:
Dr. Wayne A. Sarasua, Committee Chair
Dr. Jennifer H. Ogle
Dr. William J. Davis
Dr. Joseph M. Burgett
Dr. Christopher J. Post

ABSTRACT

Roadway safety is a multifaceted issue affected by several variables including geometric design features of the roadway, weather conditions, sight distance issues, user behavior, and pavement surface condition. In recent years, transportation agencies have demonstrated a growing interest in utilizing Light Detecting and Ranging (LiDAR) and other remote sensing technologies to enhance data collection productivity, safety, and facilitate the development of strategies to maintain and improve existing roadway infrastructure. Studies have shown that three-dimensional (3D) point clouds acquired using mobile LiDAR systems are highly accurate, dense, and have numerous applications in transportation. Point cloud data applications include extraction of roadway geometry features, asset management, as-built documentation, and maintenance operations. Another source of highly accurate 3D data in the form of point clouds is close-range aerial photogrammetry using unmanned aerial vehicle (UAV) systems. One of the main advantages of these systems over conventional surveying methods is the ability to obtain accurate continuous data in a timely manner. Traditional surveying techniques allow for the collection of road surface data only at specified intervals. Point clouds from LiDAR and imagery-based data can be imported into modeling and design software to create a virtual representation of constructed roadways using 3D models.

From a roadway safety assessment standpoint, mobile LiDAR scanning (MLS) systems and UAV close-range photogrammetry (UAV-CRP) can be used as effective methods to produce accurate digital representations of existing roadways for various safety evaluations. This research used LiDAR data collected by five vendors and UAV imagery

data collected by the research team to achieve the following objectives: a) evaluate the accuracy of point clouds from MLS and UAV imagery data for collection roadway cross slopes for system-wide cross slope verification; b) evaluate the accuracy of as-built geometry features extracted from MLS and UAV imagery-based point clouds for estimating design speeds on horizontal and vertical curves of existing roadways; c) Determine whether MLS and UAV imagery-based point clouds can be used to produce accurate road surface models for material volume estimation purposes. Ground truth data collected using manual field survey measurements were used to validate the results of this research.

Cross slope measurements were extracted from ten randomly selected stations along a 4-lane roadway. This resulted in a total of 42 cross slope measurements per data set including measurements from left turn lanes. The roadway is an urban parkway classified as an urban principal arterial located in Anderson, South Carolina. A comparison of measurements from point clouds and measurements from field survey data using t-test statical analysis showed that deviations between field survey data and MLS and UAV imagery-based point clouds were within the acceptable range of ±0.2% specified by SHRP2 and the South Carolina Department of Transportation (SCDOT).

A surface-to-surface method was used to compute and compare material volumes between terrain models from MLS and UAV imagery-based point clouds and a terrain model from field survey data. The field survey data consisted of 424 points collected manually at sixty-nine 100-ft stations over the 1.3-mile study area. The average difference in height for all MLS data was less than 1 inch except for one of the vendors which

appeared to be due to a systematic error. The average height difference for the UAV imagery-based data was approximately 1.02 inches. The relatively small errors indicated that these data sets can be used to obtain reliable material volume estimates.

Lastly, MLS and UAV imagery-based point clouds were used to obtain horizontal curve radii and superelevation data to estimate design speeds on horizontal curves. Results from paired t-test statistical analyses using a 95% confidence level showed that geometry data extracted from point clouds can be used to obtain realistic estimates of design speeds on horizontal curves. Similarly, road grade and sight distance were obtained from point clouds for design speed estimation on crest and sag vertical curves. A similar approach using a paired t-test statistical analysis at a 95% confidence level showed that point clouds can be used to obtain reliable design speed information on crest and sag vertical curves. The proposed approach offers advantages over extracting information from design drawings which may provide an inaccurate representation of the as-built roadway.

Keywords: Roadway Safety, Roadway Design, Mobile LiDAR, Unmanned Aerial Vehicle, Close-Range Photogrammetry, Roadway Geometry, As-Built Data, SHRP2.

DEDICATION

This dissertation is dedicated to my mother and late father, Maria and Capemba Cassule. I am forever appreciative of their sacrifices, love, and unwavering support.

ACKNOWLEDGMENTS

I would like to thank my advisor, Dr. Wayne Sarasua, for his invaluable support, trust, and guidance. I am immensely grateful to him for his willingness to serve as my advisor and for his leadership. I would also like to express my deepest appreciation to my committee members: Dr. Jennifer Ogle, Dr. W. Jeff Davis, Dr. Joe Burgett, and Dr. Christopher Post. Their knowledge, support, and feedback had a huge influence on the direction of my doctoral work.

I gratefully acknowledge the South Carolina Department of Transportation (SCDOT) and the Federal Highway Administration (FHWA) for supporting and funding the project that served as the basis for the studies included in this dissertation.

I am grateful to Dr. Joe Bible and all of my colleagues for their efforts and valuable contributions. I also thank Kristi Baker, Sandi Priddy, and the entire staff of the Glenn Department of Civil Engineering for their professionalism and dedication.

A special thank you goes to my family. To my wife, Y.J. “Amy”, and daughter, Angela, thank you for the love and support you have given me throughout this journey. To my parents, my siblings, and uncle Albino, thank you for the constant encouragement and for always believing in me. I would not be where I am today without your support.

Lastly, I would like to thank Stephen, Afshin, Nassim, David, Chris, Kelly, and all of my colleagues and friends who made this academic journey a memorable experience.

TABLE OF CONTENTS

Table of Contents (Continued) Page

LIST OF TABLES

List of Tables (Continued)

Table Page

LIST OF FIGURES

List of Figures (Continued)

Figure Page

CHAPTER ONE

INTRODUCTION

Light Detection and Ranging (LiDAR) is an emerging technology that can be used to obtain accurate three-dimensional (3D) information in the form of point clouds that has the potential to transform the way in which transportation agencies and service providers plan, design, build and maintain highway systems (1). Point clouds can be imported into 3D modeling software to help visualize and build a virtual representation of finished construction projects (2). The technology to support data collection using LiDAR surveys is well established and continues to evolve to integrate new advances in hardware and software (3). A review of the literature shows that much work has been done to calibrate LiDAR systems for accurate surveying (4–11). LiDAR datasets can be obtained in a variety of ways using static, mobile, and aerial systems. Many state transportation agencies are using some form of LiDAR technology because of its many benefits including data collection productivity, enhanced safety, cost-effectiveness, and technological improvement (12).

Though effective, LiDAR systems tend to be expensive and require a certain level of expertise and training to be deployed efficiently. Close-range photogrammetry (CRP) is a cost-effective and easy-to-use technology that could potentially serve as an alternative to LiDAR systems (13). Unmanned aerial systems (UAS)-based close range photogrammetry can be used to acquire and process 2D imagery data using Structure from Motion (SfM) software to generate accurate 3D point clouds. Based on principles similar to those of

traditional photogrammetry, SfM is a technique that uses advanced digital image-matching algorithms to generate high-resolution 3D point clouds, 3D reality meshes, orthophotos and digital surface models (14).

Problem Statement

Mobile LiDAR scanning (MLS) technology and close-range photogrammetry (CRP) can provide highly accurate 3D point clouds that have numerous applications in transportation. These systems can be used to overcome limitations presented by conventional surveying techniques and static LiDAR systems, particularly in terms of personnel safety, data collection efficiency, accuracy, and cost-effectiveness (13, 15).

To comply with pragmatic performance measures and performance-based funding, state transportation agencies have been using innovative and practical methods and technologies to manage roadway assets (3). MLS (1) and CRP (13) point clouds can be used to obtain common roadway geometry and asset information including grades, slopes, lane widths, and signs inventory for visibility and other safety analyses. Up-to-date and reliable information is crucial for evaluating and prioritizing new or improvement roadway projects (16). LiDAR technology has been implemented in the transportation field for safety and mobility analyses to identify sight distance obstructions and assess traffic operations while minimizing lane closures, traffic disruptions, and safety hazards (12). Lidar-based and image-based point clouds offer opportunities to develop advanced geospatial datasets to support asset management in a safe and efficient manner (17).

Advances in computer vision algorithms to extract key features from unmanned aerial vehicle (UAV)-based videos and images have prompted investigations to assess the

applications of UAVs in roadway safety, traffic engineering, and highway infrastructure management (18, 19). Similar to LiDAR, UAV-CRP technology, typically accomplished by using an optical camera mounted on a UAV platform and supported by a global navigation satellite system (GNSS) device to collect quality data, can be used for monitoring transportation infrastructure assets (20). Additionally, research studies have attempted to use CRP as an alternative and less-expensive technology for 3D pavement distress surveying (21), and to measure pavement texture characteristics and predict pavement friction with promising results (22).

This dissertation research provides a basis for evaluating the feasibility and effectiveness of using Light Detection and Ranging (LiDAR) technology and Unmanned Aerial Vehicle (UAV) photogrammetry to extract accurate as-built horizontal and vertical roadway geometry and cross-sectional geometric parameters for roadway safety evaluations, and to obtain accurate pavement material volume estimates for resurfacing and rehabilitation purposes. Accurate pavement cross-section information is essential to ensuring that roadways have adequate cross-slopes to enhance driver safety, thus minimizing the potential for hydroplaning. Having accurate details of critical as-built geometric elements and pavement surface data will ensure that appropriate warnings are properly used, design standards are met, and timely and adequate maintenance and rehabilitation operations are performed. Lastly, this research is intended to investigate whether UAV photogrammetry can be used as an efficient and accurate alternative to mobile LiDAR systems.

Research Objectives

The overall goal of this research was to conduct a technical evaluation of multiple mobile LiDAR scanning (MLS) systems and close-range photogrammetry (CRP) to determine if accurate three-dimensional (3D) surface models and as-built horizontal and vertical alignment information can be extracted using LiDAR and Imagery-based point clouds for specific safety and pavement material volume estimation applications. A detailed description of each research objective is presented below.

Description of Research Objectives:

- Evaluate if accurate cross-slope measurements can be extracted from point-cloud-based 3D surface models, and whether MLS and CRP data can be used for system-wide verification of highway cross slopes.
- Compare curve design speeds estimated using horizontal alignment parameters extracted from point clouds, and whether MLS and UAV photogrammetry data can be used for system-wide verification of design speeds on horizontal curves.
- Determine whether LiDAR and Imagery-based point clouds can be used to estimate sight distance and design speeds on vertical curves.
- In comparison with traditional surveying, investigate whether MLS and imagery-based point clouds can be used to produce accurate road surfaces to estimate pavement material volumes for pavement resurfacing and rehabilitation.

To achieve these research objectives, mobile LiDAR and UAV imagery data sets were collected on a roadway test section located in Anderson, South Carolina. Conventional survey measurements collected using high accuracy GPS units, total stations, and leveling were used as ground truth data for comparison purposes.

Content and Organization of Dissertation

This dissertation document consists of three research papers on roadway cross slope measurement, extraction of horizontal and vertical roadway geometry for design speed evaluations, and pavement material volume estimation for resurfacing and rehabilitation purposes using LiDAR and UAV photogrammetry data sets. Each research paper represents one chapter of the dissertation. The data sets used in the three studies were collected using the same data collection systems and methods.

PAPER I: A COMPARISON OF MOBILE LIDAR AND LOW-ALTITUDE UNMANNED AERIAL VEHICLE PHOTOGRAMMETRY FOR COLLECTING HIGHWAY CROSS SLOPE MEASUREMENTS

OBJECTIVES

- Develop and implement a practical semi-automated workflow using modeling software to extract cross-slope information from LiDAR and close-range photogrammetry data.
- Conduct a technical evaluation of the accuracy of Mobile LiDAR and UVA photogrammetry for system-wide verification of highway cross slopes.

- Identify and highlight benefits and recommendations based on technical evaluations.

PAPER II: ROADWAY PAVEMENT MATERIAL VOLUME ESTIMATION FOR RESURFACING AND REHABILITATION USING MOBILE LIDAR AND IMAGERY-BASED POINT CLOUDS

OBJECTIVES

- Evaluate the accuracy of surfaces terrain models created using mobile LiDAR and UAV imagery-based point clouds.
- Determine if accurate pavement material volume estimates can be made for resurfacing and rehabilitation purposes and compare results to manual survey methods.

PAPER III: SAFETY ASSESSMENT OF DESIGN SPEED ON HORIZONTAL AND VERTICAL CURVES USING MOBILE LIDAR AND UNMANNED AERIAL VEHICLE PHOTOGRAMMETRY

OBJECTIVES

- Develop a feasible approach to extract horizontal curve geometry features including tangent length, curve radius, point of curvature, point of intersection, point of tangency, curve length, and middle ordinate distance.
- Develop a feasible approach to extract vertical alignment features including longitudinal grades, vertical point of curvature, vertical point of intersection, vertical point of tangency, and curve length.

- Evaluate grade measurement deviations based on recommended accuracy values specified by SHRP2.
- Calculate design speeds on horizontal and vertical curves using geometry features extracted from point clouds.

REFERENCES

1. Olsen, M. J. Guidelines for the Use of Mobile LIDAR in Transportation Applications. Transportation Research Board, 2013.
2. Schneider, C. (FHWA). 3D, 4D, and 5D Engineered Models for Construction. 2013.
3. Federal Highway Administration (FHWA). Guide for Efficient Geospatial Data Acquisition Using LiDAR Surveying Technology. 2016.
4. Glennie, C. Rigorous 3D Error Analysis of Kinematic Scanning LIDAR Systems. JOURNAL OF APPLIED GEODESY 1 (3) , pp.147-157, 2007, p. pp.147.
5. Barber, D., J. Mills, and S. Smith-Voysey. Geometric Validation of a Ground-Based Mobile Laser Scanning System. ISPRS JOURNAL OF PHOTOGRAMMETRY AND REMOTE SENSING, Vol. 63, No. 1, 2008, pp. 128–141. https://doi.org/10.1016/j.isprsjprs.2007.07.005.
6. Haala, N., M. Peter, J. Kremer, and G. Hunter. Mobile LiDAR Mapping for 3D Point Cloud Collection in Urban Areas—A Performance Test. Int. Arch. Photogramm. Remote Sens. Spat. Inf. Sci, Vol. 37, 2008, pp. 1119–1127.

7. Habib, A., K. I. Bang, A. P. Kersting, and J. Chow. Alternative Methodologies for LiDAR System Calibration. REMOTE SENSING, Vol. 2, No. 3, 2010, pp. 874–907. https://doi.org/10.3390/rs2030874.

8. Siying, C., M. Hongchao, Z. Yinchao, Z. Liang, X. Jixian, and C. He. Boresight Calibration of Airborne LiDAR System Without Ground Control Points. IEEE GEOSCIENCE AND REMOTE SENSING LETTERS, Vol. 9, No. 1, 2012, pp. 85–89. https://doi.org/10.1109/LGRS.2011.2161070.

9. Shi, S., S. Song, W. Gong, L. Du, B. Zhu, and X. Huang. Improving Backscatter Intensity Calibration for Multispectral LiDAR. IEEE GEOSCIENCE AND REMOTE SENSING LETTERS, Vol. 12, No. 7, 2015, pp. 1421–1425. https://doi.org/10.1109/LGRS.2015.2405573.

10. Pusztai, Z., I. Eichhardt, and L. Hajder. Accurate Calibration of Multi-LiDAR-Multi-Camera Systems. SENSORS, Vol. 18, No. 7, 2018. https://doi.org/10.3390/s18072139.

11. Ravi, R., Y.-J. Lin, M. Elbahnasawy, T. Shamseldin, and A. Habib. Simultaneous System Calibration of a Multi-LiDAR Multicamera Mobile Mapping Platform. IEEE JOURNAL OF SELECTED TOPICS IN APPLIED EARTH OBSERVATIONS AND REMOTE SENSING, Vol. 11, No. 5, 2018, pp. 1694–1714. https://doi.org/10.1109/JSTARS.2018.2812796.

12. Chang, J. C., D. J. Findley, C. M. Cunningham, and M. K. Tsai. Considerations for Effective Lidar Deployment by Transportation Agencies. TRANSPORTATION RESEARCH RECORD, No. 2440, 2014, pp. 1–8. https://doi.org/10.3141/2440-01.

13. Cross, C., M. Farhadmanesh, and A. Rashidi. Assessing Close-Range Photogrammetry as an Alternative for LiDAR Technology at UDOT Divisions. Utah. Dept. of Transportation. Division of Research, 2020.

14. Kessler, M. L. Advanced Geospatial Tools. FHWA-HRT-19-004. Vol. 83 No. 2. https://highways.dot.gov/public-roads/summer-2019/advanced-geospatial-tools.

15. Williams, K., M. J. Olsen, G. V. Roe, and C. Glennie. Synthesis of Transportation Applications of Mobile LIDAR. Remote Sensing, Vol. 5, No. 9, 2013, pp. 4652–4692. https://doi.org/10.3390/rs5094652.

16. Ural, S., J. Shan, M. A. Romero, and A. Tarko. ROAD AND ROADSIDE FEATURE EXTRACTION USING IMAGERY AND LIDAR DATA FOR TRANSPORTATION OPERATION. No. 2–3, Stilla, U and Heipke, C, ed., 2015, pp. 239–246.

17. Roe, G. V, M. S. O'Banion, and M. J. Olsen. Mobile Lidar Guidelines to Support Utility Asset Management along Highways. 2016.

18. Barmpounakis, E. N., E. I. Vlahogianni, and J. C. Golias. Unmanned Aerial Aircraft Systems for Transportation Engineering: Current Practice and Future Challenges. International Journal of Transportation Science and Technology, Vol. 5, No. 3, 2016, pp. 111–122.

19. Outay, F., H. A. Mengash, and M. Adnan. Applications of Unmanned Aerial Vehicle (UAV) in Road Safety, Traffic and Highway Infrastructure Management: Recent Advances and Challenges. Transportation research part A: policy and practice, Vol. 141, 2020, pp. 116–129.

20. Congress, S. S. C., A. J. Puppala, and C. L. Lundberg. Total System Error Analysis of UAV-CRP Technology for Monitoring Transportation Infrastructure Assets. ENGINEERING GEOLOGY, Vol. 247, 2018, pp. 104–116. https://doi.org/10.1016/j.enggeo.2018.11.002.

21. Ahmed, M., C. T. Haas, and R. Haas. Toward Low-Cost 3D Automatic Pavement Distress Surveying: The Close Range Photogrammetry Approach. CANADIAN JOURNAL OF CIVIL ENGINEERING, Vol. 38, No. 12, 2011, pp. 1301–1313. https://doi.org/10.1139/L11-088.

22. Al-Assi, M., E. Kassem, and R. Nielsen. Using Close-Range Photogrammetry to Measure Pavement Texture Characteristics and Predict Pavement Friction. TRANSPORTATION RESEARCH RECORD, Vol. 2674, No. 10, 2020, pp. 794–805. https://doi.org/10.1177/0361198120936650.

CHAPTER TWO

PAPER I: A COMPARISON OF MOBILE LIDAR AND LOW-ALTITUDE UNMANNED AERIAL VEHICLE PHOTOGRAMMETRY FOR COLLECTING HIGHWAY CROSS SLOPE MEASUREMENTS

Abstract

The purpose of sloping roadway cross sections is to ensure adequate drainage of water. The accumulation of water can lead to hydroplaning or other problems, which can increase crashes. The most common methods for identifying inadequate cross slope are through visual inspection of poor drainage and crash occurrence. Ideally, a proactive approach of identifying roadway sections of inadequate cross slope to reduce crash

potential is preferred over reacting to problem locations where crashes may occur. Some states use traditional field surveying techniques and other manual measurement methods to collect cross slope data on a limited basis. These methods do not provide continuous data, are labor intensive, and expose personnel to traffic hazards. This study conducted a technical evaluation of Unmanned Aerial Vehicle (UAV) Photogrammetry, and Mobile LiDAR Scanning (MLS) systems for effectiveness in measuring pavement cross slopes. Four MLS vendors were invited to participate in a demonstration rodeo where LiDAR data were collected along a 1.4-mile section of a 4-lane, 3-mile parkway located in Anderson County, South Carolina. Additionally, the research team collected UAV stereo imagery along the same roadway section. Cross-slope data were extracted from LiDAR point clouds using a semi-automated workflow in OpenRoads Designer (ORD). The observed means of absolute measurement errors were 0.146% for mobile LiDAR, and 0.148% for UAV photogrammetry. Results indicated that MLS and UAV photogrammetry performed comparably and provided reliable results for cross slope determination.

Keywords: Mobile LiDAR, Cross-Slope, Hydroplaning, UAV Photogrammetry

Introduction

Proper surface drainage is an important consideration in the design of highways. Improper roadway drainage may interrupt traffic, reduce skid resistance, and increase the potential for hydroplaning (1). Water drainage from the pavement surface is dependent on longitudinal grade, cross slope, pavement width, surface texture, and rainfall intensity (2). Although longitudinal grade may have a considerable effect on flow path length, it does not appreciably affect pavement water depth (2, 3). Cross slope has a substantial impact on

pavement water depth because it helps to drain water laterally and minimizes ponding (4). Well-designed cross-slopes can provide sufficient drainage while minimizing the risk of vehicles drifting or skidding laterally when braking (5). Paved roads are commonly designed and constructed with careful consideration given to the correct shape of the finished cross section (6).

Through crash history and field surveys, the South Carolina Department of Transportation (SCDOT) has identified isolated sections of interstate freeway that have substandard cross slopes for proper drainage. This observational approach suggests that there is a likelihood that significant mileage of South Carolina highways may not have sufficient cross slope to ensure proper drainage. South Carolina currently does not have a program to conduct large-scale inspections of cross slopes. This type of limitation is not unusual. A survey of state highway agencies across the U.S. determined that while 70% collected some cross slope data, none did so on a system-wide basis. Most of the states surveyed performed cross slope verification only on Interstate and primary routes, and only at locations with apparent drainage problems or at locations that experience a high number of weather-related crashes (4, 7). Survey responses indicated distinct interest in identifying technology that can be used to efficiently collect pavement cross slope data on a wide scale basis.

Currently, conventional surveying techniques or other manual methods are used to collect cross slope data in most states at selected locations. Conventional surveying and other manual methods are labor-intensive, expose personnel to traffic, and cause delays to the traveling public (8). Furthermore, conventional surveying for cross slope verification

purposes can only be conducted at sample locations and may not be representative of segments between the samples (4). SCDOT's emphasis on ensuring that adequate pavement cross slopes are maintained through verification is predicated upon two principles: 1) deployment of a safe and efficient method for collecting cross slope data; and 2) adoption occurs system-wide so an accurate and comprehensive network-based cross slope database can be maintained (7).

Aerial photogrammetry has been used for topographic ground surveying for highway projects for more than 50 years (9). Elevations derived from photogrammetry are dependent on flying height and camera quality and are less accurate than conventional ground surveys. Estimating cross slopes from photogrammetry-based contour maps has not been viable because of accuracy issues related to the minimum altitudes that planes can fly at. Close-range Unmanned Aerial Vehicle (UAV) photogrammetry can potentially produce cross slope data at sufficient accuracy for verification purposes because of low flying heights and use of high-resolution cameras.

Light Detection and Ranging (LiDAR) systems can provide highly accurate georeferenced three-dimensional data that have numerous applications in transportation. The adoption of mobile LiDAR technology by transportation agencies has significantly increased over the past decade. Mobile LiDAR Scanning (MLS) systems provide significant safety and efficiency advantages over conventional surveying techniques and static LiDAR scanning systems when collecting data. The data processing workflow of MLS requires the processing of positional data alongside LiDAR data (10).

The researchers previously studied MLS and Aerial (airplane mounted) LiDAR approaches to collect cross slope data with promising results (11). This paper evaluates close-range unmanned aerial vehicle (UAV) photogrammetry collection of highway cross slopes. A comparison with conventional surveying and MLS is provided.

Literature Review

Photogrammetry Applications

Aerial photogrammetry is the science of locating three-dimensional points from two or more images. Aerial photogrammetry plays an important part in highway location and design, especially in preparing existing ground contour maps. A review of the literature indicates that cross slope measurements from aerial photographs are not currently practiced. This is due to the scale of aerial photographs, which is a function of flying height. The highest accuracy standards for aerial photogrammetry data are in the 0.25 ft horizontal and vertical accuracy classes (12). These accuracy classes are associated with an RMSE of 0.25 ft. While this error tolerance is suitable for highway alignment design and earthwork calculations, the associated relative accuracy is not accurate enough for collecting reliable highway cross-slope data. One type of aerial photogrammetry that can potentially provide the needed accuracy for collecting cross slope data is close-range photogrammetry (CRP). Traditional photogrammetry requires flying heights of greater than 1000 ft, equating to the minimum safe flying height above populated areas, as required by the FAA. Small UAVs are able to fly significantly lower than 1000 ft and collect much higher resolution images.

UAV Photogrammetry

Burgett et al. investigated whether the use of commercially available UAVs and software could create surveys to be used for preconstruction surveys. Their study acquired data at three altitudes and three separate times using two common commercial UAVs. Results of their study indicated that survey points could be within 0.68 cm (0.022 ft) horizontally, 0.09 cm (0.003 ft) in elevation, and 1.46 cm (0.048 ft) in three dimensions (3D) of the true location (13).

Similarly, Aguera-Vega et al. studied the accuracy of drone-based surveys. The authors evaluated the influence of flight altitude, terrain morphology, and the number of ground control points (GCPs) on the digital surface model (DSM) and orthoimage accuracies obtained from UAV photogrammetry (14). The authors compared 60 photogrammetric models based on five terrain morphologies, four flight altitudes, and three different numbers of GCPs. The study used a rotary wing platform UAV with eight motors and a nonmetric mirrorless reflex camera. Results of their study indicated the following: the number of GCPs influenced the horizontal accuracy; as GCPs increased, accuracy improved; vertical accuracy was not influenced by terrain morphology; vertical accuracy decreased as flight altitude increased. Accuracies of 0.053 m (0.17 ft) horizontally and 0.079 m (0.26 ft) vertically were obtained using a flight altitude of 50 m (164 ft) and 10 GCPs.

Road condition assessment is an important task in road maintenance (15). (Zhang and Elaksher, 2012) evaluated the use a UAV-based digital imaging system to collect

surface condition data over rural roads. The authors used aerial imagery data to derive a three-dimensional surface model for road distress measurement. Results of their investigation showed that the difference between 3D information measurements and onsite manual measurements of road distresses was around half a centimeter (0.0164 ft).

LiDAR Technology

Research studies have identified several benefits associated with the implementation of LiDAR technology and how transportation agencies can potentially use LiDAR systems to plan, design, inspect, and maintain transportation infrastructure. In recent years, state transportation agencies have shown an increased interest in LiDAR technology due to its practical uses in transportation; and for being potentially more cost-effective than traditional surveying technologies (16). Additionally, recent studies have discussed the potential benefits of using LiDAR to extract lane markings (17, 18), evaluate pavement friction (19), and extract and assess road geometry (20, 21).

A study by Shams et al. provided an evaluation of MLS systems in terms of the accuracy and precision of collected cross-slope data, including documentation of procedures necessary to calibrate, collect, and process LiDAR data (4). MLS data were collected by five different vendors on three roadway sections. The sample data obtained allowed estimation of 95% confidence intervals for true mean absolute deviations of cross slopes from manual survey measurements to be 0.10% to 0.19% which is within SHRP2 specifications of acceptable margin of error (22).

Gargoum et al. attempted to extract road cross sections from LiDAR data. Their study proposed an algorithm that involved estimating vectors intersecting the road's axis whereby points within proximity to the vectors were retained and extracted (23). Slope information was measured based on the retained points. The authors used multivariate adaptive regression splines (MARS) to identify points of inflection or change in slope. Linear regression was used to estimate the slopes between points of inflection which represented cross slopes and side slopes of the extracted cross section. Cross slopes estimated using the proposed procedure were compared to slope data collected in GPS surveys. Percent differences ranged from 0.0001% to 0.4% for the 38 cross slopes estimated.

Gurganusa et al. proposed a method to evaluate hydroplaning potential based on the actual road surface and geometric properties measured using MLS (24). The authors used a single mobile LiDAR system to measure surface geometry, and a Monte Carlo simulation to produce a traveling speed at which hydroplaning could occur. Their investigation showed that MLS could provide distance data within 0.15% of the ground truth distance. An in-service roadway with historical wet weather crashes was used in their investigation. The authors concluded that the traveling speed at which hydroplaning could occur was lower than the posted speed limit.

Ai and Tsai proposed an automated sidewalk assessment method using three-dimensional mobile LiDAR and image processing. Features regulated by the Americans with Disabilities Act (ADA), including sidewalk width, cross slope, grade, and curb ramp slope were automatically measured and compared with manual ground truth data from a

field survey (25). The proposed mobile system consisted of video cameras, two mobile LiDAR systems, and a global navigation system. Sidewalks were extracted from the LiDAR point cloud using a roadway segmentation method. Results of their investigation showed that measurements derived from the proposed method were close to ground truth measurements. The absolute error in the sidewalk width measurements was less than 0.15 m (0.5 ft), and less than 0.2% slope measurement errors were observed at 20 randomly selected locations.

Luo and Li used a mobile mapping system consisting of an inertial measurement unit (IMU), GPS, a distance measuring indicator (DMI), and a 3D LiDAR system to automatically measure highway ramp geometry (26). Pavement slopes were calibrated using an inertial measurement unit (IMU) and transverse profile data. Additionally, a validation test was conducted using field measurements. The average errors for curve detection and curve radius measurements were 5.89 and 1.99%, respectively. P-values for longitudinal and cross-slope measurements were 0.621 and 0.989, respectively. The authors suggested the proposed method could be used for roadway surveys.

The quantitative assessment of LiDAR elevation data is usually conducted by comparing high-accuracy control points with elevations estimated from LiDAR ground data (27). Liu argued that the vertical accuracy with respect to a specified datum is critical in determining the accuracy of LiDAR data. In addition to exploring the performance of various methods for deriving elevations from LiDAR, the authors used survey markers to assess the vertical accuracy of LiDAR data for different land covers. Results of their study

indicated the suitability of using survey markers as checkpoints to assess the vertical accuracy of LiDAR data (24).

Tsai et al. discussed the need for transportation agencies to identify and measure road sections that have noneffective cross slopes so that timely corrective maintenance could be performed. Their investigation proposed a mobile cross-slope measurement method using LiDAR technology to conduct network-level cross slope measurement at highway speeds (28). Components of their method included a mobile LiDAR system, high-resolution video cameras, a GPS unit, an inertial measurement unit, and a distance measurement instrument. Results from a controlled test showed that their method achieved desirable accuracy with an average measurement difference of less than 0.13% cross-slope from the digital level measurements with standard deviations within 0.05% in three runs at all benchmarked locations.

All of the LiDAR studies cited in this section focusing on slope measurements are MLS based. No previous studies were identified that evaluated UAV photogrammetry to collect cross slope data.

Study Area and Data Collection

This research evaluated the use of UAV photogrammetry compared to mobile LiDAR to collect cross slope data along a 1.4-mile section of four-lane parkway located in Anderson, South Carolina. East West Parkway begins at US-76 (Clemson Boulevard) and ends at SC-81. Ten stations from locations with distinct roadway slope characteristics (normal crown and superelevated) and different lane geometry were randomly selected along the corridor for cross slope evaluation test sections. A ground control survey was

performed to identify ground control points (GCPs), shown in Figure 2-1. The study area was surveyed to locate 100 ft stations along the white edge lines. Stations were marked with PK surveying nails including the yellow centerline markings. Reflective pavement marking tape was placed at the PK nails located on the white edge lines to ensure that PK nail locations could be identified in the LiDAR point clouds using the intensity or RGB color attributes within point clouds. Lane markings were identified based on intensity and RGB attributes. A ground control survey was performed to establish primary and secondary GCPs throughout the study area. Primary and secondary GCPs served as a means of tying down data sets for consistent comparison.

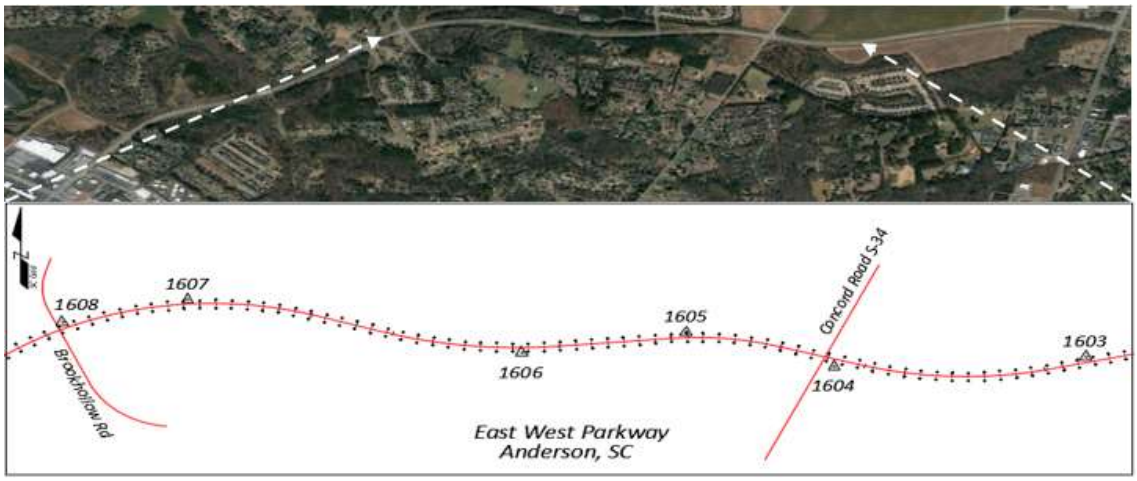

Figure 2-1 GCPs and station locations along the 1.4-mile study area.

Mobile LiDAR Data Collection

MLS data were collected in the summer of 2016. Four different MLS vendors used a minimum of two primary GCPs as base station locations for GPS differential correction of the MLS data. Additional GCPs were used for post-processing least-squares adjustment of the LiDAR point clouds. Vendors were asked to collect MLS data in two directions from

the right (outer) lane while driving at the posted speed limit. Most mobile LiDAR systems can collect accurate point cloud data for multiple travel lanes with a single pass from either travel lane along a corridor. Vendors provided their respective equipment specifications, which are provided in Table 2-1. Decisions regarding equipment calibration were made by vendors individually. That is, equipment calibrations were performed both before and after data collection runs. Traffic control was provided for the MLS data collection by two trailing SCDOT vehicles without obstructing the opposing travel direction.

Photogrammetry Data Collection

UAV photogrammetry data were collected on March 19, 2021. The UAV photogrammetry data collection process was considerably less labor intensive compared to MLS data collection. The research team used a commercially available UAV, with a 20mp imager with a retail value of $2,500. The specifications of the UAV system are provided in Table 2-1. Data were collected at two elevations (117 ft and 288 ft AGL) to improve scene coverage and provide two vertical planes to triangulate elevations. A total of 358 images were collected at 117 ft, and 380 images were collected at 288 ft. Bentley's ContextCapture is a structure-from-motion photogrammetry package commonly used by practitioners and some state DOTs. In this study, ContextCapture was used to process the 2D georeferenced images into a 3D point cloud. The 3D point cloud was exported and compared with MSL data in OpenRoads Designer. The accuracy of the points was improved using four geolocated GCPs. The GCPs reduce the RMS error in the point cloud and improve accuracy with precise scaling. The average ground resolution of the collected

imagery data was 22.2679 mm/pixel. Figure 2-2 provides a graphical representation of the scene coverage of overlapping images. On average, 24 images were used to compute the location of each point in the point cloud. However, because the lane lines were in the center of the scene, those points were calculated using approximately 35 images per point.

Table 2-1. Overview of Equipment Specifications

Data Type	Source	Brand	Model	Type	Measurement Rate
Mobile LiDAR	Vendor A	Riegl	VMX 450	Dual laser	1100 KHz
	Vendor B	Teledyne Optech	MI	Dual laser	500 KHz/Sensor
	Vendor C	Teledyne Optech	SGI	Dual laser	600 KHz/Sensor
	Vendor D	Z+F Profiler	9012	Single laser	1000 KHz
Photogrammetry	UAV Phantom 4 Pro	DJI	Phantom 4 Pro	Sensor: 1" CMOS	Mechanical Shutter Speed 8 - 1/2000s Electronic Shutter Speed 8 - 1/8000s

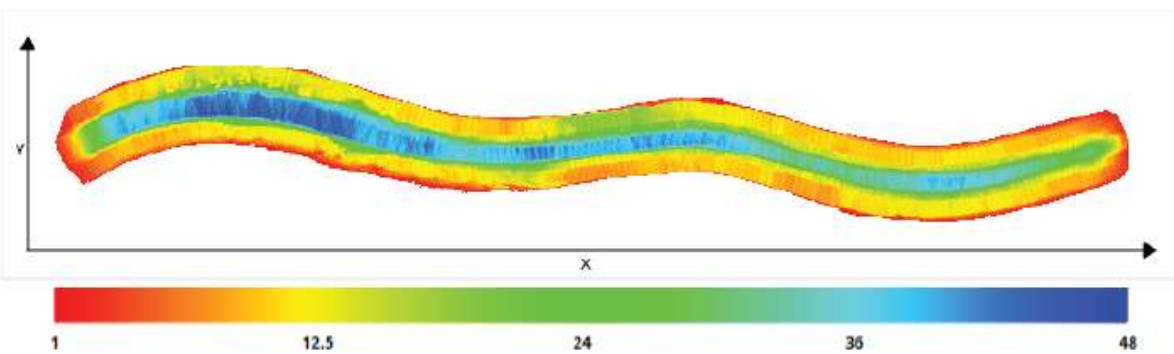

Figure 2-2 Photo density: Top view (XY plane) display of the scene with colors indicating the number of photos that potentially see each area.

Cross Slope Extraction from Point Cloud Data

Data collected at two altitudes were combined before cross slope measurements were extracted. A multistep semi-automated method was used to extract cross slope

information from the LiDAR and photogrammetry-based point clouds. Edge of pavement, lane lines, and centerlines were identifiable in the MLS and UAV photogrammetry point cloud data using intensity and RGB color attributes, respectively. Bentley Systems' OpenRoads Designer (ORD) clip tools were used to remove points beyond the white edge lines, and non-ground points that were not automatically classified within point clouds. To define the cross-section line at selected test sections, a 4-in cross-sectional buffer of points was defined and semi-automatically clipped based on the width of the reflective pavement marking tape that points to the PK surveying nails on the white edge lines. Next, a reference line was drawn through the clipped buffer of points between the two PK nail locations identified in ORD as shown in Figure 2-3. The clipped points were used to create a surface terrain model (STM) using ORD terrain modeling tools. Specifically, an ORD tiling algorithm, which is a divide and conquer recursive algorithm that divides the data into tiles, was used to filter the data and fit a plane through each tile within the point cloud using a Z tolerance value of 0.012-in. The variation in the Z coordinate that the surface can move during the filtering process is controlled by the specified Z tolerance value. The reference line projected along the buffered surface is used to extract cross slope data in a semi-automated fashion based on the rise and run between pavement markings, shown in Figure 2-4. This process was repeated for all test locations (n=42) across each of the ten randomly selected stations.

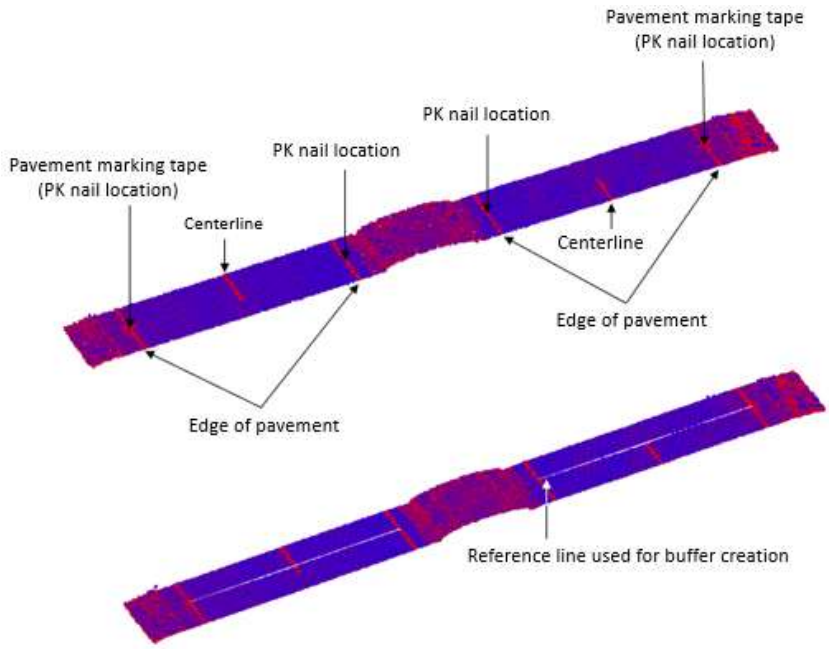

Figure 2-4 Identification of pavement markings and cross-section reference line.

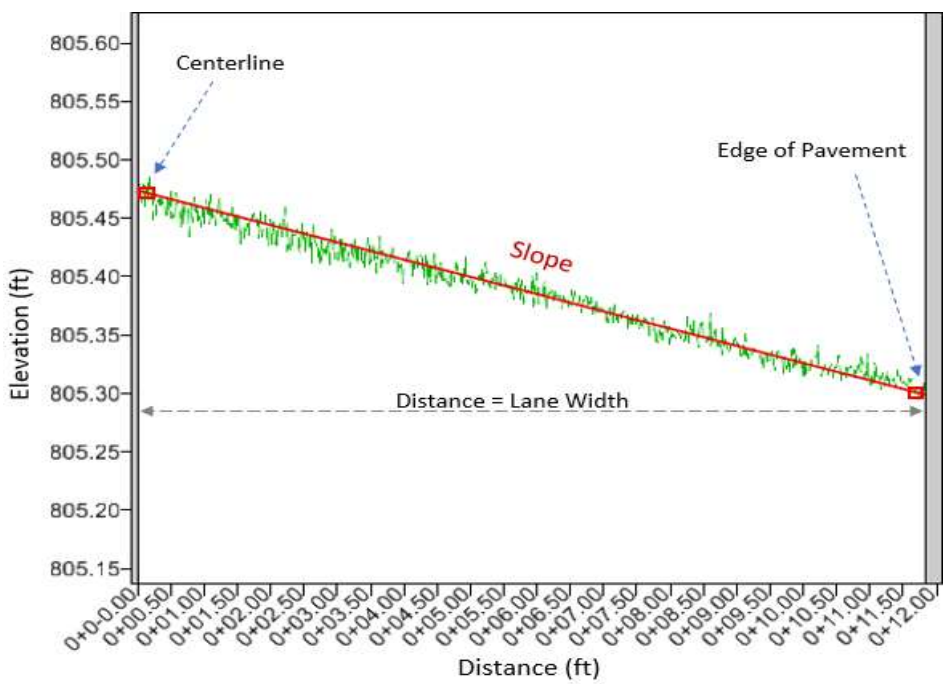

Figure 2-3 Example of cross slope extraction from point cloud data using a surface terrain model based on a cross-sectional buffer of points.

Evaluation of Results

Results of this investigation are presented in Table 2-2 and Table 2-3. Travel lanes were labeled as follows: EBO = Eastbound Outer, EBI= Eastbound Inner, WBI = Westbound Inner, WBO = Westbound Outer, and LTL = Left Turn Lane. Cross-slope measurements collected using conventional surveying techniques and the difference between field survey data and measurements extracted from point cloud data are shown in Table 2-2. That is, the values shown under vendors and UAV photogrammetry represent deviations in percent from the manually surveyed measurements which served as ground truth data.

Table 2-2 Comparison between Cross Slope Measurements Derived from Manual Survey, Mobile LiDAR, and UAV Photogrammetry data.

				Difference between measurements (absolute value) Field survey cross slope - Extracted measurement				
				Vendors				UAV Photogrammetry
Station	Lane	Lane Width (HD)	Field Survey cross slope (Ground truth)	A	B	C	D	
170+00	EBO	11.57	3.83%	0.16%	0.02%	0.03%	0.02%	0.01%
	EBI	12.09	3.89%	0.02%	0.03%	0.05%	0.12%	0.36%
	WBI	11.89	2.99%	0.14%	0.23%	0.14%	0.27%	0.17%
	WBO	11.61	3.73%	0.02%	0.11%	0.03%	0.30%	0.09%
173+00	EBO	11.69	3.49%	0.16%	0.18%	0.09%	0.19%	0.26%
	EBI	12.15	3.04%	0.00%	0.12%	0.01%	0.00%	0.08%
	WBI	11.88	3.32%	0.25%	0.05%	0.07%	0.50%	0.29%
	WBO	11.43	3.88%	0.02%	0.12%	0.06%	0.24%	0.10%
175+00	EBO	11.40	3.88%	0.02%	0.28%	0.14%	0.24%	0.18%
	EBI	12.24	3.11%	0.16%	0.20%	0.17%	0.35%	0.28%
	WBI	11.34	3.33%	0.03%	0.11%	0.02%	0.64%	0.60%
	WBO	11.59	4.29%	0.21%	0.22%	0.15%	0.50%	0.01%

190+00	EBO	12.02	3.00%	0.00%	0.13%	0.07%	0.03%	0.30%
	EBI	11.60	2.32%	0.30%	0.07%	0.27%	0.27%	0.21%
	WBI	11.66	2.86%	0.10%	0.11%	0.10%	0.21%	0.03%
	WBO	12.30	2.92%	0.24%	0.41%	0.13%	0.04%	0.59%
198+00	EBO	11.63	1.91%	0.23%	0.05%	0.01%	0.05%	0.21%
	EBI	11.57	3.04%	0.10%	0.00%	0.04%	0.01%	0.07%
	WBI	11.37	0.80%	0.40%	0.06%	0.07%	0.12%	0.08%
	WBO	11.45	0.18%	0.16%	0.08%	0.02%	0.13%	0.12%
203+00	EBO	11.94	3.81%	0.09%	0.22%	0.02%	0.37%	0.03%
	EBI	11.83	4.65%	0.08%	0.02%	0.04%	0.40%	0.06%
	WBI	11.57	3.59%	0.07%	0.50%	0.09%	0.06%	0.06%
	WBO	11.86	4.60%	0.06%	0.46%	0.00%	0.10%	0.12%
208+00	EBO	11.62	2.32%	0.28%	0.08%	0.07%	0.15%	0.09%
	EBI	11.88	2.48%	0.17%	0.06%	0.06%	0.31%	0.16%
	LTL	12	2.01%	0.30%	0.01%	0.06%	0.20%	0.00%
	WBI	11.90	1.09%	0.06%	0.34%	0.15%	0.14%	0.12%
	WBO	11.42	0.00%	0.24%	0.12%	0.00%	0.03%	0.18%
212+00	EBO	11.56	1.08%	0.13%	0.07%	0.12%	0.19%	0.08%
	EBI	11.69	1.75%	0.13%	0.35%	0.04%	0.38%	0.06%
	LTL	10.27	2.26%	0.04%	0.36%	0.11%	0.02%	0.19%
	WBI	12.34	2.86%	0.13%	0.11%	0.14%	0.22%	0.01%
	WBO	11.48	1.31%	0.34%	0.01%	0.18%	0.01%	0.00%
220+00	EBO	11.73	3.42%	0.13%	0.09%	0.06%	0.00%	0.30%
	EBI	11.58	2.54%	0.02%	0.01%	0.05%	0.03%	0.20%
	WBI	11.43	4.43%	0.02%	0.17%	0.16%	0.34%	0.00%
	WBO	11.68	3.61%	0.13%	0.11%	0.10%	0.29%	0.01%
227+00	EBO	11.73	2.39%	0.00%	0.29%	0.03%	0.03%	0.02%
	EBI	12.13	2.14%	0.03%	0.37%	0.00%	0.06%	0.25%
	WBI	11.81	1.91%	0.98%	*	*	0.32%	0.21%
	WBO	11.95	1.88%	0.04%	0.32%	0.01%	0.38%	0.01%

*Missing data; HD = Horizontal distance (ft)

Comparison of UAV Photogrammetry and MLS survey data

The methodology used to extract pavement cross-slope information from MLS and UAV photogrammetry point clouds was designed to mimic the traditional surveying approach for comparison purposes. To evaluate the dispersion of observed values with

respect to ground truth measurements, mean absolute errors (MAE) were calculated. This was performed as the first step in the comparative analysis. The observed MAEs for measurements obtained from MLS and photogrammetry data sets were 0.146%, and 0.148%, respectively. Mean absolute errors were calculated using the following equation:

$$MAE = \frac{1}{n}\sum_{i=1}^{n}|d_{ai} - d_{oi}| = \frac{1}{n}\sum_{i=1}^{n}|e_i| \quad (2\text{-}1)$$

Where:

n= Number of observations

d_{ai}= Manually surveyed measurement

d_{oi}= Observed value (extracted measurement)

$|e_i|$= Absolute difference between surveyed and observed measurements

Standard deviations (SD) were calculated to evaluate the spread of estimated measurements with respect to the mean. SD values for MLS and photogrammetry data sets were 0.14% and 0.14%, respectively. Standard deviations were calculated using the following equation:

$$SD = \sqrt{\frac{\sum_{i=1}^{n}|d_{oi} - \overline{d_a}|^2}{n-1}} \quad (2\text{-}2)$$

Where:

d_{o_i} = Observed value (extracted measurement)

$\overline{d_a}$ = Expected value (Manually surveyed measurement)

n = Number of observations

A summary of cross slope measurement comparisons is shown in table 2-3.

Table 2-3 Summary of Cross-Slope Measurement Comparisons

		EB Outer Lane	EB Inner Lane	Turning Lane	WB Inner Lane	WB Outer Lane
Mobile LiDAR	Min	0.00%	0.00%	0.00%	0.02%	0.00%
	Max	0.37%	0.40%	0.69%	0.98%	0.50%
	Mean	0.11%	0.12%	0.21%	0.20%	0.15%
	Median	0.09%	0.06%	0.15%	0.14%	0.12%
	One sided t-test	t_{obs}	df	p-value	Significant	
	$H_a: \mu < 0.2$	-4.83	165	<0.01	Yes	
UAV Photogrammetry	Min	0.01%	0.06%	0.00%	0.00%	0.00%
	Max	0.30%	0.36%	0.19%	0.60%	0.59%
	Mean	0.15%	0.17%	0.09%	0.16%	0.12%
	Median	0.14%	0.18%	0.09%	0.10%	0.09%
	One sided t-test	t_{obs}	df	p-value	Significant	
	$H_a: \mu < 0.2$	-2.38	41	=0.02	Yes	

Discussion

The means of the errors of measurements extracted from MLS data sets were between 0.11% and 0.21% with a mean absolute error (MAE) of 0.146%, and standard deviation of 0.14%. The means of the errors of measurements extracted from photogrammetry point clouds were between 0.09% and 0.17% with a mean absolute error of 0.148% and standard deviation of 0.14%. Overall, MLS and photogrammetry results were within the acceptable range of ±0.2% specified by SHRP 2 and SCDOT. In fact, both the means and variances for the MLS and UAV samples tested to be equal with $t_{obs} = -.05\ on\ df = 206, p = .95$, and $F_{obs} = 1.01\ on\ df_1 = 165\ and\ df_2 = 41, p = .97$, respectively. Based on these findings we conclude that UAV photogrammetry performs at least as well, on average as the MLS systems.

It is noteworthy that MAE for each MLS vendor varied by vendor. Table 2-4 summarizes the MAE values for each of the MLS vendors. The photogrammetry values are included for comparison purposes. The average MAE for all lanes ranged from 0.075% for vendor C to 0.197% for vendor D. All of the vendor LiDAR systems had similar sampling rates and similar published accuracy specifications. Some of the vendors collected their data on different days which can affect GPS positions depending on PDOP value at the time of data collection. Other factors that can influence MLS accuracy are the inertial measurement unit and equipment calibration. The evaluated values for all roadway lanes within the study area meet the SHRP 2 specification (±0.2%), with the exception of a few of the individual lane MAE values that are greater than 0.2%.

Another observation of note is that MLS data is better for outer lanes compared to inner lanes in most cases. This is to be expected because the MLS vendors were asked to drive in the outer lane during the data collection, thus the data in the outer lane is collected at a closer range at an angle nearly perpendicular to the LiDAR sensor.

Table 2-4 MAE Values by Lane from MLS and UAV Photogrammetry Data

Lane	Vendors				UAV Photogrammetry
	A	B	C	D	
EBO	0.120%	0.141%	0.064%	0.127%	0.148%
EBI	0.101%	0.123%	0.073%	0.193%	0.173%
WBI	0.218%	0.187%	0.104%	0.282%	0.157%
WBO	0.146%	0.196%	0.068%	0.202%	0.123%
All lanes	0.147%	0.162%	0.077%	0.197%	0.148%

Conclusion

This study conducted a technical evaluation of close-range UAV photogrammetry and multiple MLS systems. The use of MLS and UAV photogrammetry for cross slope measurements were evaluated at ten stations along a designated test section of East West Parkway in Anderson, South Carolina. The results of this study showed that both MLS and UAV photogrammetry derived cross slopes are comparable to conventional manual survey measurements. The observed MAEs for MLS ranged from 0.077% to 0.197% with an overall average of 0.15% and 0.15% for UAV photogrammetry. Results indicated that MLS and UAV photogrammetry provided accurate results for cross slope determination.

Conventional surveying methods are time consuming and require a survey crew to collect data within the roadway limits, which presents safety issues and may interfere with traffic. LiDAR scanning and photogrammetry platforms can be used to capture cross slopes, grades, and a variety of other geometric design characteristics efficiently. These applications can increase productivity, minimize road crew exposure, and create reliable continuous data sets of roadway information that can serve multiple uses beyond cross slope measurement, such as highway asset management.

REFERENCES

1. AASHTO. Highway Drainage Guideline. American Association of the State Highway and Transportation Officials (AASHTO), Washington D.C, 2007.

2. Guven, O., and J. Melville. PAVEMENT CROSS SLOPE DESIGN - A TECHNICAL REVIEW. Auburn University. 1999, p. 29.

3. Gallaway, B. M., R. E. Schiller, and J. G. Rose. The Effects of Rainfall Intensity, Pavement Cross Slope, Surface Texture, and Drainage Length on Pavement Water Depths. 1971.

4. Shams, A., W. A. Sarasua, A. Famili, W. J. Davis, J. H. Ogle, L. Cassule, and A. Mammadrahimli. Highway Cross-Slope Measurement Using Mobile LiDAR. Transportation Research Record, Vol. 2672, No. 39, 2018. https://doi.org/10.1177/0361198118756371.

5. AASHTO. A Policy on Geometric Design of Highways and Streets. American Association of State Highway and Transportation Officials, Washington D.C, 2011.

6. FHWA. Gravel Roads Construction and Maintenance Guide. Vol. FHWA-OTS-, 2015, p. 153.

7. Sarasua, W. A., W. Davis, and J. H. O. Cross Slope Verification Using Mobile Scanning on SCDOT Highways. South Carolina Department of Transportation (SCDOT). Publication FHWA-SC-18-07. South Carolina Department of Transportation (SCDOT), Columbia, SC, 2018.

8. Yen, K. S., B. Ravani, and T. A. L. LiDAR for Data Efficiency. Washington (State). Dept. of Transportation. Office of Research and Library Services, 2011.

9. HRB. AERIAL SURVEYS AND USES OF PHOTOGRAMMETRY FOR HIGHWAYS. Special Report 81, Highway Research Board, 1964.

10. Williams, K., M. J. Olsen, G. V. Roe, and C. Glennie. Synthesis of Transportation Applications of Mobile LIDAR. Remote Sensing, Vol. 5, No. 9, 2013, pp. 4652–4692. https://doi.org/10.3390/rs5094652.

11. Shams, A., W. A. Sarasua, B. T. Russell, W. J. Davis, C. Post, H. Rastiveis, A. Famili, and L. Cassule. Extracting Highway Cross Slopes From Airborne and Mobile LiDAR Point Clouds. Transportation Research Record, 2022, p. 03611981221106482.

12. ASPRS. ASPRS Positional Accuracy Standards for Digital Geospatial Data. Photogrammetric Engineering & Remote Sensing, 2014.

13. Burgett, J., B. Lytle, D. Bausman, S. Shaffer, and E. Stuckey. Accuracy of Drone-Based Surveys: Structured Evaluation of a UAS-Based Land Survey. JOURNAL OF INFRASTRUCTURE SYSTEMS, Vol. 27, No. 2, 2021. https://doi.org/10.1061/(ASCE)IS.1943-555X.0000605.

14. Aguera-Vega, F., F. Carvajal-Ramirez, and P. Martinez-Carricondo. Accuracy of Digital Surface Models and Orthophotos Derived from Unmanned Aerial Vehicle Photogrammetry. JOURNAL OF SURVEYING ENGINEERING, Vol. 143, No. 2, 2017. https://doi.org/10.1061/(ASCE)SU.1943-5428.0000206.

15. Zhang, C. S., and A. Elaksher. An Unmanned Aerial Vehicle-Based Imaging System for 3D Measurement of Unpaved Road Surface Distresses. COMPUTER-AIDED CIVIL AND INFRASTRUCTURE ENGINEERING, Vol. 27, No. 2, 2012, pp. 118–129. https://doi.org/10.1111/j.1467-8667.2011.00727.x.

16. Chang, J. C., D. J. Findley, C. M. Cunningham, and M. K. Tsai. Considerations for Effective Lidar Deployment by Transportation Agencies. TRANSPORTATION RESEARCH RECORD, No. 2440, 2014, pp. 1–8. https://doi.org/10.3141/2440-01.

17. Guan, H., J. Li, Y. Yu, C. Wang, M. Chapman, and B. Yang. Using Mobile Laser Scanning Data for Automated Extraction of Road Markings. ISPRS Journal of Photogrammetry and Remote Sensing, Vol. 87, 2014. https://doi.org/10.1016/j.isprsjprs.2013.11.005.

18. Ma, L., T. Wu, Y. Li, J. Li, Y. Chen, and M. Chapman. Automated Extraction of Driving Lines from Mobile Laser Scanning Point Clouds. Advances in Cartography and GIScience of the ICA, Vol. 1, 2019, pp. 1–6. https://doi.org/10.5194/ica-adv-1-12-2019.

19. Du, Y. C., Y. S. Li, S. C. Jiang, and Y. Shen. Mobile Light Detection and Ranging for Automated Pavement Friction Estimation. TRANSPORTATION RESEARCH RECORD, Vol. 2673, No. 10, 2019, pp. 663–672. https://doi.org/10.1177/0361198119847610.

20. Holgado-Barco, A., D. Gonzalez-Aguilera, P. Arias-Sanchez, and J. Martinez-Sanchez. An Automated Approach to Vertical Road Characterisation Using Mobile LiDAR Systems: Longitudinal Profiles and Cross-Sections. ISPRS JOURNAL OF PHOTOGRAMMETRY AND REMOTE SENSING, Vol. 96, 2014, pp. 28–37. https://doi.org/10.1016/j.isprsjprs.2014.06.017.

21. Shalkamy, A., L. Karsten, S. Gargoum, and K. El-Basyouny. A Framework to Detect Horizontal Curves and Assess Their Geometric Properties from Remotely

Sensed Point Clouds. INTERNATIONAL JOURNAL OF REMOTE SENSING, Vol. 41, No. 21, 2020, pp. 8328–8351. https://doi.org/10.1080/01431161.2020.1771792.

22. Hunt, J. E., A. Vandervalk, and D. S. SHRP2 Report S2-S03-RW-01: Roadway Measurement System Evaluation. Transportation Research Board of the National Academies, Washington, D.C., 2013.

23. Gargoum, S. A., K. El-Basyouny, K. Froese, and A. Gadowski. A Fully Automated Approach to Extract and Assess Road Cross Sections From Mobile LiDAR Data. IEEE TRANSACTIONS ON INTELLIGENT TRANSPORTATION SYSTEMS, Vol. 19, No. 11, 2018, pp. 3507–3516. https://doi.org/10.1109/TITS.2017.2784623.

24. Gurganusa, C. F., S. Chang, and N. G. Gharaibeh. Evaluation of Hydroplaning Potential Using Mobile Lidar Measurements for Network-Level Pavement Management Applications. ROAD MATERIALS AND PAVEMENT DESIGN, 2021. https://doi.org/10.1080/14680629.2021.1899962.

25. Ai, C. B., and Y. C. Tsai. Automated Sidewalk Assessment Method for Americans with Disabilities Act Compliance Using Three-Dimensional Mobile Lidar. TRANSPORTATION RESEARCH RECORD, No. 2542, 2016, pp. 25–32. https://doi.org/10.3141/2542-04.

26. Luo, W., and L. Li. Automatic Geometry Measurement for Curved Ramps Using Inertial Measurement Unit and 3D LiDAR System. Automation in Construction, Vol. 94, 2018. https://doi.org/10.1016/j.autcon.2018.07.004.

27. Liu, X. Accuracy Assessment of Lidar Elevation Data Using Survey Marks. Survey Review, Vol. 43, No. 319, 2011, pp. 80–93. https://doi.org/10.1179/003962611X12894696204704.

28. Tsai, Y., C. Ai, Z. Wang, and E. Pitts. Mobile Cross-Slope Measurement Method Using Lidar Technology. Transportation Research Record, No. 2367, 2013. https://doi.org/10.3141/2367-06.

CHAPTER THREE

PAPER II: ROADWAY PAVEMENT MATERIAL VOLUME ESTIMATION FOR RESURFACING AND REHABILITATION USING MOBILE LIDAR AND IMAGERY-BASED POINT CLOUDS

Abstract

Innovative data acquisition technologies allow state transportation agencies and industry practitioners more flexibility to develop efficient and cost-effective workflows for roadway maintenance, design, and asset management. Transportation agencies perform resurfacing, rehabilitation, and maintenance tasks on an ongoing basis. Hence, road construction, rehabilitation, and resurfacing project costs incurred by transportation agencies result in thousands of dollars per mile each year. Accurate methods for estimating material quantities are crucial in providing reliable estimates and minimizing costs. Light Detection and Ranging (LiDAR) and Unmanned Aerial Vehicle (UVA) photogrammetry systems can be used to obtain large datasets of accurate, high-density three-dimensional point clouds. Point cloud data can be used to obtain detailed information representing the existing ground as well as design and as-built surfaces for earthwork and surface material

volume calculation purposes. In this study, pavement material volume quantities were calculated using terrain models created from LiDAR point clouds collected by five vendors, and terrain models created from UAV photogrammetry and manual survey data collected by the research team. Volume differences were due to variations in the surfaces obtained using each point cloud data set. Additionally, terrain models generated using mobile LiDAR scanning (MLS), and UAV photogrammetry-based point clouds were compared based on calculated earthwork volume quantities between terrain models. Volume quantities were calculated using a surface-to-surface method in OpenRoads Designer. A 1.3-mile section along an urban parkway located in Anderson County, South Carolina was used as the testbed to investigate the differences between road surface terrain models generated using mobile LiDAR and imagery-based point clouds. The average difference in height between surfaces ranged from 0.17 inches between two MLS vendor surfaces to 1.67 inches between UAV photogrammetry and one of the MLS vendors.

Keywords: Earthwork, Mobile LiDAR, UAV Photogrammetry, Pavement rehabilitation and resurfacing, Surface Modeling.

Introduction

Emerging technologies such as mobile LiDAR scanning (MLS) and unmanned aerial vehicle (UVA) photogrammetry can be used to collect large data sets of the characteristics of roadway surfaces along corridors in the form of a point cloud. These datasets facilitate the creation of workflows to extract accurate three-dimensional (3D)

models of roadways in a timely manner. The use of 3D models has the potential to accelerate construction operations, reduce costs, improve accuracy, and enhance safety during construction operations (1). Hence, various phases of the road construction process can benefit from these technologies including data collection, data processing, cost estimating, and design phases. Modeling software can be used to process LiDAR and UVA photogrammetry data sets to create accurate 3D terrain models representing existing ground, design, and as-built surfaces that can be used to estimate material volumes. Earthwork is commonly defined as the process of excavating, hauling, and placing soil and other earthen materials during construction projects (2, 3). Efficient management of earthwork operations requires, among other things, accurate estimating of volume quantities (3). Earthwork volume quantities represent the total amount of soil or other pavement material to be transported to and from a construction site. Cut and fill volumes are known as the amount of material to be removed (cut) or placed (fill) to reach a desired elevation or grade. Methods typically used to calculate earthwork volume quantities for road construction projects include the traditional average-end-area calculations based on cross sections, and surface to surface computations to determine cut and fill volumes. Average-end-area volumes are based on the sum of volumes of the prismoids formed by adjacent cross sections (4). Surface to surface computations, enabled by modeling software, can be used to determine volumes between two terrain models based on the union of the terrain models (see Fig. 3-1).

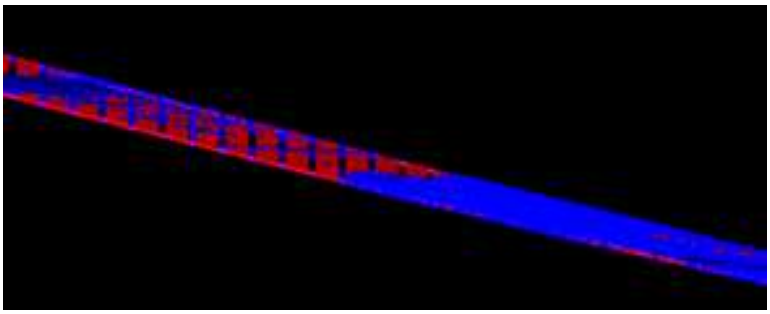

Figure 3-1 Example of earthwork volume computation based on the union of two terrain models (surface-to-surface method).

Traditional surveying techniques allow for the collection of surface data only at specified intervals. While this approach is accurate enough for most applications including repaving, pavement maintenance, and quantity estimating; dense and continuous data sets such as point clouds from survey-grade systems provide a more accurate representation of the topography of the surface to be modeled. Having an accurate representation of the surface topography is critical to obtaining accurate volume quantities. Inaccurate pavement material estimates may lead to undesirable consequences during construction including costly contractor change orders. MLS, and UAV photogrammetry data sets consist of highly accurate three-dimensional point clouds that provide high-density continuous data. Continuous data sets provide more detailed three-dimensional information than conventional surveying methods that rely on data collected at specified cross-sectional intervals. This study evaluated the use of mobile LiDAR and UVA photogrammetry point cloud data to compute pavement material volume quantities. Comparisons were made with survey data collected manually by the research team. MLS data sets were collected by four vendors invited to participate in the study. Because the exact same section of road was used

for data collection, a perfect surface in all cases should result in zero cut, zero fill, and zero net volume when doing the comparisons. Comparisons in close agreement with low material quantity estimates between surfaces indicates the point clouds used in the comparison accurately reflect the actual surface and can be used for performing volume estimates. This study aims to facilitate the decision-making process regarding technologies and surveying approaches that may be used for specific projects.

Literature Review

Many studies have explored the feasibility of using LiDAR and UAV photogrammetry data for road surface modeling purposes. These modern technologies can be deployed in small study areas as well as in wide multilane corridors. The literature shows various approaches investigating the accuracy of LiDAR and UVA photogrammetry terrain models.

LiDAR Technology Applications

Modern laser scanning data collection technologies are becoming increasingly popular for being potentially more cost-effective than conventional surveying techniques. Mobile Terrestrial LiDAR and aerial LiDAR systems are at the forefront of this trend. Recent studies have investigated advantages associated with the implementation of LiDAR technology by transportation agencies (5). Data collection productivity, enhanced safety, cost-effectiveness, and improved accuracy are among the primary benefits associated with the increasing adoption of LiDAR technology (6).

LiDAR surveys enable practitioners to perform rapid and accurate data collection and facilitate the consolidation of resources and maximization of available funding (7). Due to its applicability in the transportation industry, a growing number of transportation agencies have acquired some form of LiDAR technology in recent years. Besides providing the ability to generate terrain models with a high degree of accuracy, LiDAR data sets can be used to perform a variety of road safety analyses including assessment of road pavement condition. De Blasiis et al. (8) took advantage of the dense point clouds acquired using mobile laser systems (MLS) to identify pavement degradations that affect safety, namely potholes and shoving in the pavement surface. Ravi et al. (9) proposed an automated approach for pavement surface inspection based on an algorithm capable of analyzing pavement surface models generated from mobile mapping system (MMS) point clouds acquired at highway speeds of approximately 60 mph. The authors suggested that their approach could detect anomalies as small as 2 cm in the form of cracking, potholes, and surface debris. Li et al. (10) attempted to use unmanned aerial vehicle (UAV) LiDAR to rapidly and accurately extract different types of pavement distress due to natural and human factors. Efficient pavement management systems depend on accurate, reliable, and complete data on pavement conditions (11), which can be accomplished with LiDAR technology.

Unmanned Aerial Vehicle (UAV) Photogrammetry Applications

Unmanned Aerial Vehicle (UVA) photogrammetry can provide benefits similar to those obtained with LiDAR systems including cost-effectiveness, data collection

efficiency, and enhanced safety. Previous studies have identified UVAs as a valuable source of image data for 3D reconstruction of man-made structures (12–14).

Uysal et al. (15) described UAV photogrammetry as a low-cost, less time-consuming, and sufficiently accurate alternative to traditional surveying approaches. Similarly, Tan and Li (16) argued that unmanned aerial vehicles (UAVs) represent an excellent option for road condition monitoring. The authors used road images from UAV oblique photogrammetry for image reconstruction to generate 3D models from which pavement distresses were automatically detected and extracted.

Farhadmanesh et al. (17) investigated the feasibility of using LiDAR and photogrammetry systems to monitor highway assets and pavement condition. Al-Assi et al. (18) explored the suitability of using close-range photogrammetry (CRP) to generate 3D models to measure pavement macro texture and micro texture. Their approach involved processing stereo images using digital photogrammetric software to generate 3D surface models.

A study by Khanal et al. (19) investigated the accuracy of mobile terrestrial LiDAR, aerial LiDAR, and UAV photogrammetry data sets collected over different terrain types by comparing elevations obtained from each data source with conventionally surveyed data. The researchers concluded that data collected using either technology can be used for road design as well as reconstruction and rehabilitation of existing roadways. These approaches indicated that UAV photogrammetry can potentially be used to ensure timely and proper resurfacing and rehabilitation of damaged roadways.

Calibration of LiDAR and UAV Photogrammetry systems

A critical aspect regarding the implementation of LiDAR and UVA photogrammetry technology in transportation for accurate surveying is that systems be properly calibrated. Commercial software packages can be used to post-process Global Navigation Satellate System (GNSS) and Inertial Measurement Unit (IMU) data along with ground-based LiDAR scans to obtain accurate point clouds (20). A review of the literature shows various efforts and methodologies to calibrate LiDAR and UVA photogrammetry systems with and without ground control points (21–24).

Barber et al. (25) evaluated the precision and accuracy of a ground-based mobile mapping system using conventionally surveyed check points. The authors performed an estimate of the system's precision using repeated data collection passes. Results of their investigation indicated a measurement precision between 0.029 m and 0.031 m in elevation, planimetric accuracy of approximately 0.10 m, and RMS errors in elevation in the order of 0.03 m.

Ravi et al. (26) proposed a calibration procedure for both airborne and terrestrial mobile mapping systems that estimates the mounting parameters for several spinning multibeam laser scanners and cameras on board a LiDAR platform. Their results indicated that for the UAV-based laser scanning unit used in the study, the processing accuracy in position was between 2 cm and 5 cm. The car-mounted mobile laser scanning system provided an accurary of approximately 3 cm for the derived point cloud coordinates at a range of 30 m.

Glennie (27) investigated the overall 3D expected error accuracy of LiDAR systems using a rigorous first order error analysis of the LiDAR georeferencing equations. The authors evaluated common error parameters as well as the expected horizontal and vertical system accuracies for different LiDAR systems.

Furthermore, studies have identified close-range photogrammetry as a potential alternative to LiDAR scanning devices and manual data collection approaches (28). Luhman et al. (29) presented a review of aspects of sensor modeling and camera calibration for close-range photogrammetry with a focus on techniques of automated self-calibration. Similarly, Gabrlik at al. (30) proposed a multi-sensor system for direct georeferencing of UAV-based aerial imagery and validated results using a high number of test points.

Earthwork Estimation Approaches

The two most common methods used to compute earthwork quantities in transportation applications are 1) the average-end-area (AEA) method and 2) the surface-to-surface method. The ability to obtain accurate earthwork quantities has been significantly enhanced by modern data collection and processing technologies that can be used to generate, overlay, and compare 3D surfaces models to obtain earthwork volumes. In recent years, state transportation agencies have increasingly used three-dimensional (3D) models to plan and design roadways due to benefits such as improved productivity, accuracy, and worker safety during construction operations (31).

The conventional way of determining earthwork quantities is to use the average-end-area method. The AEA method involves establishing survey cross-sections along the

roadway at regular intervals from which cut and fill volume quantities are estimated (32). Research studies have suggested that many state transportation agencies and practitioners still use or specify the average-end-area method for calculating earthwork volume quantities for road construction projects (2). Because volume quantities are calculated between cross-sections, the average end-area method is labor intensive and difficult to apply when the construction consists of nonlinear sections (33). The average-end-area method calculates earthwork volumes between consecutives cross sections by multiplying the average of the two cross sectional end areas (A1 and A2) by the perpendicular distance between the cross sections (L). The AEA method is given by the following equation:

$$V = \frac{1}{2}(A_1 + A_2) * L \tag{3-1}$$

Schexnayder and Mayo (34) argued that the AEA method gives volume results that are slightly in excess of the actual volume, with a precision of about ±1%. Additionally, the authors suggested that although 100-ft stations are typically used when the project is linear in extent and the ground surface is regular, measurements should be taken at closer intervals (less than 100 ft), when the surface irregular, particularly at points of change. The accuracy of earthwork computations is directly affected by the extent and accuracy of field measurements.

Hintz and Vonderohe (2) compared volumes computed using the average-end-area method with surface-to-surface volume quantities calculations using modeling software. Their investigation showed that end-area volumes approached those computed by surface-

to-surface calculations when the cross-section interval was reduced. Additionally, the authors argued that variations could be due to random variability of the terrain.

Similarly, Slattery and Slattery (35) argued that the AEA method is unreliable in sections that change from cut and fill and where the construction consists of non-linear sections. The authors evaluated the feasibility of using terrestrial laser scans on roadway construction projects as an efficient approach to measure earthwork quantities. Their study indicated that results could be improved using measurement methods that provide more dense data such as 3D mobile terrestrial laser scanning.

Study Area and Data Collection

The study area is a 1.3-mile section of a relatively recently built 4-lane urban roadway (East West Parkway) located in Anderson County, SC, shown in Figure 3-2. Geometric features of the study area include linear sections, four horizontal curves, five vertical curves, and two lanes in each direction.

Figure 3-2 Stations and GCP locations along the study area: Anderson, SC (East West Parkway)

Data were collected in three phases. The research team performed a ground control survey to identify ground control points (GCPs) throughout the study area (see Fig. 3-3). Existing geodetic survey marks were used as primary ground control points. Primary and secondary GCPs provided a means for tying down data sets for consistent comparison. Similarly, the research team performed a survey to establish 100-ft stations along the edges of the travel lanes (see Fig 3-4).

Figure 3-3 Sample primary and secondary control points used to adjust LiDAR and photogrammetry data sets.

Figure 3-4 Reflective pavement marking tape used to identify survey stations along the white pavement edge lines.

Equipment used during the traditional data collection process include total stations, smart levels, and high-accuracy GPS units. To facilitate the identification of stations and GCPs using point cloud intensity and RGB color attributes, reflective pavement marking tape was placed at station markers along the white pavement edge lines on both sides of the roadway.

Mobile LiDAR datasets were collected by industry vendor using their own LiDAR systems and survey crews. Vendors were provided with traffic control support consisting of two trailing SCDOT vehicles and were instructed to collected data using the right (outer)

lane while traveling at the posted speed limit (see Fig. 3-5). Vehicles in the opposing travel direction were allowed to move without obstruction. All LiDAR datasets were collected using one pass in each direction because most mobile LiDAR systems can collect accurate data for multiple lanes from either lane along a roadway as shown in Figure 3-6. LiDAR equipment were calibrated by vendors before and after each data collection pass. Vendors were responsible for ensuring that LiDAR systems were calibrated throughout the data collection process.

Figure 3-5 Mobile Lidar data collection. (SCDOT traffic control trucks and sample LiDAR system and vehicle used by vendors).

Figure 3-6 Sample Mobile LiDAR scan from the outer (right) lane.

The research team collected aerial imagery data using a commercially available UAV with a retail value of approximately $2,500, (see Fig 3-7). The detailed specifications of the systems are presented in Table 3-1. The UAV photogrammetry data acquisition process was conducted as follows: a) Identification of GCP locations within the study area, b) Placement of aerial survey targets, c) Flight planning, d) Equipment calibration and image data acquisition, e) Data processing for 3D information extraction. Data were collected using two elevations to enhance scene coverage. That is, imagery data were collected in two directions, eastbound (EB) and westbound (WB), at 117 ft and 288 ft AGL relative to the point of takeoff. The two elevations provided two vertical planes to triangulate elevations. In total, 358 and 380 images were collected at altitudes of 117 ft and 288 ft, respectively. Images were georeferenced using control points. Three-dimensional point clouds were generated using images collected at both altitudes. The unmanned aerial system used to collect imagery data is shown in figure 3-7. Figure 3-8 shows a point cloud generated using UAV imagery data.

Figure 3-7 Unmanned aerial system used to collect imagery data.

Figure 3-8 Three-dimensional point cloud from collected UAV imagery data.

Equipment specifications provided by vendors, as well as equipment used by the research team are summarized in Table 3-1.

Table 3-1 Mobile Lidar and UAV Photogrammetry Equipment Specifications

Data Collection Method	Source of Data	Brand Name	Model	Type	Measurement Rate
MLS	Vendor A	Riegl	VMX 450	Dual laser	1100 KHz
	Vendor B	Teledyne Optech	MI	Dual laser	500 KHz/Sensor
	Vendor C	Teledyne Optech	SGI	Dual laser	600 KHz/Sensor
	Vendor D	Z+F Profiler	9012	Single laser	1000 KHz
	Vendor E	Teledyne Optech	MI	Dual laser	500 KHz/Sensor
UAV Photogrammetry	Commercially Available UAV	DJI	Phantom 4 Pro	Sensor: 1" CMOS	Mechanical Shutter Speed 8 - 1/2000s Electronic Shutter Speed 8 - 1/8000s

Analysis Methodology

Primary and secondary ground control points (GCPs) were used to georeference data sets using a common coordinate system. MLS point clouds were adjusted through

post-processing with ground control points. The research team used four GCPs to adjust the UVA photogrammetry data. ContextCapture, a Bentley's structure-from-motion software package commonly used by practitioners and some state DOTs, was used to process the 2D georeferenced images into a 3D point cloud. Four geolocated ground control points (GCPs) were used for tying down point cloud data for consistent comparison. The location of each point within the point cloud was computed using between 24 and 35 images, on average. The average ground resolution of the images collected was 22.2679 mm/pixel.

Prior to the creation of terrain models, LiDAR and UAV photogrammetry point clouds were processed in OpenRoads Designer to remove noises from the data; that is, non-ground points created by power lines, vegetation, and other small obstacles located in the median and shoulders were removed. Point clouds were clipped directionally between the white pavement edge lines before the data were filtered so that accurate terrain models could be generated. Typically, point clouds should be filtered to remove existing scatter points from the surface generated due to random measurement errors (35). Two lanes in each direction were kept and dedicated left turn lanes were removed from the analysis. Since material quantities are typically determined by actual surface area (i.e., length x width) made in the field prior to removal (36), terrain models were clipped using a predefined boundary that included both travel lanes in each direction. That is, a common boundary was used to ensure that volume quantity comparisons were not affected by variations in the planar area of terrain models created from each data set.

The conventional survey surface was generated using points manually surveyed along the white pavement edge lines and across each established station. On average, 6 points were surveyed across each station to include both travel lanes in each direction and the double yellow lines. Overall, 424 points were manually surveyed at sixty-nine 100-ft stations over the 1.3-mile study area.

Results and Discussion

Pavement Material Volume Calculations

Material volumes were calculated using a surface-to-surface method in OpenRoads Designer by setting one of the surfaces as existing and the other as the design surface. The total volume difference between the two surfaces is the same regardless of which terrain model is set as the design or existing surface. Table 3-2 shows the total volume difference (cut plus fill) in cubic yards between surface pairs including eastbound and westbound lanes. The ideal volume is zero. The table indicates that the closest comparison from a total volume standpoint is between Vendor B and Vendor C.

Table 3-2 Total Volume Difference between Surface Pairs Including Eastbound and Westbound Lanes. Units = yd^3

Terrain Model	Conventional Survey	Vendors				
		A	B	C	D	E
Conventional Survey						
Vendor A	745					
Vendor B	355	823				
Vendor C	366	872	102			
Vendor D	610	652	413	429		
Vendor E	486	1060	249	197	488	
UAV Photogrammetry	532	1287	486	448	714	291

Average perpendicular height variation between surfaces

To better understand the magnitude of the volume differences in Table 3-2, the volume differences were converted into inches in terms of perpendicular height between the surfaces. To estimate the average perpendicular height difference between two surfaces, the total volume between the surfaces was divided by the average of the planar areas. Planer areas included approximately two lanes in each direction. Thus, two lanes in each direction (24 ft) x 1.3-mile segment (6864 ft). Table 3-3, Table 3-4, and Table 3-5 show results of average perpendicular height difference calculations in inches. The ideal height difference is zero for reasons stated previously. Again, Vendor's B and C compares most favorably having the lowest average height difference in both travel directions individually and combined. The table shows that this difference is less than ¼". The average difference in heights for all of the MLS vendors is less than 1 inch except for Vendor A. The average height difference for Vendor A's results are greater than 1" difference in every comparison. Most of these differences are because of a very large cut volume compared to fill which indicates a systematic error. Because different systems and calibration methods yield different vertical and horizontal accuracies, terrain model heights may vary slightly between surface models however systematic errors should be eliminated through careful calibration and post-process least squares adjustment using ground control points. Nevertheless, even an inch of error is relatively small when considering that many contour maps used for highway purposes are created from airplane based aerial photogrammetry with flying heights greater than 1000 feet. The smallest contour interval will typically be 1 foot and error standards are that contours should be within half a contour

interval of actual which indicates acceptable differences of up to 6” in this case (37). Thus, even a 1” difference is relatively small. UAV photogrammetry average height differences range from 0.775” to 1.398”. It is noteworthy that conventional survey data in this case is not ground truth because of the 100’ interval between survey points. Thus, everything between the 100’ interval is interpolated.

Table 3-3 Eastbound Lanes: Average Height Difference between Surface Terrain Models. Units = inches.

Data Source		**Conventional Survey**	**Vendors**				
			A	**B**	**C**	**D**	**E**
Conventional Survey							
Mobile LiDAR	Vendor A	1.22					
	Vendor B	0.51	1.33				
	Vendor C	0.60	1.41	0.16			
	Vendor D	0.86	1.15	0.62	0.63		
	Vendor E	0.70	1.41	0.43	0.36	0.79	
UAV Photogrammetry		0.79	1.39	1.03	0.99	1.35	0.78

Table 3-4 Westbound Lanes: Average Height Difference between Surface Terrain Models. Units = inches.

Data Source		**Conventional Survey**	**Vendors**				
			A	**B**	**C**	**D**	**E**
Conventional Survey							
Mobile LiDAR	Vendor A	1.26					
	Vendor B	0.67	1.39				
	Vendor C	0.62	1.49	0.18			
	Vendor D	1.16	1.01	0.75	0.79		
	Vendor E	0.65	1.79	0.42	0.33	0.93	
UAV Photogrammetry		0.72	1.95	0.68	0.62	1.19	0.57

Table 3-5 Both Directions (EB and WB): Average Height Difference between Surface Terrain Models. Units = inches.

Data Source		Conventional Survey	Vendors				
			A	B	C	D	E
Conventional Survey							
Mobile LiDAR	Vendor A	1.24					
	Vendor B	0.59	1.36				
	Vendor C	0.61	1.45	0.17			
	Vendor D	1.01	1.08	0.68	0.71		
	Vendor E	0.68	1.60	0.42	0.34	0.86	
UAV Photogrammetry		0.76	1.67	0.85	0.81	1.27	0.67

Conclusions

In this study, differences between surface terrain models produced by MLS, UAV photogrammetry, and traditional survey data were compared. The established testbed location, East-West Parkway in Anderson, South Carolina, provided a study area of a typical rolling terrain multilane roadway along an urban alignment extending along a 1.3-mile parkway length. The use of MLS and UAV photogrammetry data collection methods produced similar surfaces. For both eastbound and westbound lanes of the 1.3-mile test bed study location, the average elevation differences between the MLS, UAV photogrammetry, and the traditional surveying surfaces ranges from 0.17 inches to 1.27 inches when vendor A is excluded from the comparison. These results indicate that surfaces generated from all three methods could be interchangeably used for pavement material volume estimation purposes. Thus, terrain models from MLS and imagery-based point clouds could help improve leveling course quantity estimates. However, acquiring higher spatial resolution UAV photogrammetry data and collecting additional ground control points may improve

the accuracy of pavement surface elevations. Similarly, additional noise removal may help improve the accuracy of surface terrain models generated from point clouds. The use of digital surface models to obtain accurate material volumes and project quantities would be highly beneficial to state departments of transportation in scoping, planning, designing, and administering a wide variety of roadway improvement, safety, capacity, and maintenance related projects. Accurate material volume estimates would be very helpful in providing third-party private highway contractors with accurate quantities, resulting in fewer project change orders and reduced scheduling delays.

REFERENCES

1. Schneider, C. 3D Engineered Models for Construction - Case Study for Policies and Organizational Changes for Implementation: The Kentucky Case Study. FHWA-HIF-1, 2013.
2. Hintz, C., and A. P. Vonderohe. Comparison of Earthwork Computation Methods. Transportation research record, Vol. 2215, No. 1, 2011, pp. 100–104.
3. Nunnally, S. W. Construction Methods and Management: Pearson New International Edition PDF EBook. Pearson Higher Ed, 2013.
4. Federal Highway Administration (FHWA). Project Development and Design Manual (Earthwork Design). 2022.
5. Guan, H., J. Li, S. Cao, and Y. Yu. Use of Mobile LiDAR in Road Information Inventory: A Review. International Journal of Image and Data Fusion, Vol. 7, No. 3, 2016, pp. 219–242.

6. Chang, J. C., D. J. Findley, C. M. Cunningham, and M. K. Tsai. Considerations for Effective Lidar Deployment by Transportation Agencies. TRANSPORTATION RESEARCH RECORD, No. 2440, 2014, pp. 1–8. https://doi.org/10.3141/2440-01.

7. Federal Highway Administration (FHWA). Guide for Efficient Geospatial Data Acquisition Using LiDAR Surveying Technology. 2016.

8. De Blasiis, M. R., A. Di Benedetto, and M. Fiani. Mobile Laser Scanning Data for the Evaluation of Pavement Surface Distress. Remote Sensing, Vol. 12, No. 6, 2020. https://doi.org/10.3390/rs12060942.

9. Ravi, R., D. Bullock, and A. Habib. Pavement Distress and Debris Detection Using a Mobile Mapping System with 2D Profiler LiDAR. Transportation Research Record, 2021, p. 03611981211002529.

10. Li, Z., C. Cheng, M.-P. Kwan, X. Tong, and S. Tian. Identifying Asphalt Pavement Distress Using UAV LiDAR Point Cloud Data and Random Forest Classification. ISPRS INTERNATIONAL JOURNAL OF GEO-INFORMATION, Vol. 8, No. 1, 2019. https://doi.org/10.3390/ijgi8010039.

11. Pierce, L. M., G. McGovern, and K. A. Zimmerman. Practical Guide for Quality Management of Pavement Condition Data Collection. Federal Highway Administration, 2013.

12. Wang, J., and C. Li. Acquisition of UAV Images and the Application in 3D City Modeling. No. 6623, 2008, pp. 280–290.

13. Irschara, A., V. Kaufmann, M. Klopschitz, H. Bischof, and F. Leberl. Towards Fully Automatic Photogrammetric Reconstruction Using Digital Images Taken from UAVs. 2010.

14. Remondino, F., L. Barazzetti, F. Nex, M. Scaioni, and D. Sarazzi. UAV Photogrammetry for Mapping and 3d Modeling–Current Status and Future Perspectives. International archives of the photogrammetry, remote sensing and spatial information sciences, Vol. 38, No. 1, 2011, p. C22.

15. Uysal, M., A. S. Toprak, and N. Polat. DEM Generation with UAV Photogrammetry and Accuracy Analysis in Sahitler Hill. Measurement, Vol. 73, 2015, pp. 539–543.

16. Tan, Y., and Y. Li. UAV Photogrammetry-Based 3D Road Distress Detection. ISPRS International Journal of Geo-Information, Vol. 8, No. 9, 2019. https://doi.org/10.3390/ijgi8090409.

17. Farhadmanesh, M., C. Cross, A. H. Mashhadi, A. Rashidi, and J. Wempen. Highway Asset and Pavement Condition Management Using Mobile Photogrammetry. Transportation Research Record, 2021, p. 03611981211001855.

18. Al-Assi, M., E. Kassem, and R. Nielsen. Using Close-Range Photogrammetry to Measure Pavement Texture Characteristics and Predict Pavement Friction. TRANSPORTATION RESEARCH RECORD, Vol. 2674, No. 10, 2020, pp. 794–805. https://doi.org/10.1177/0361198120936650.

19. Khanal, M., M. Hasan, N. Sterbentz, R. Johnson, and J. Weatherly. Accuracy Comparison of Aerial Lidar, Mobile-Terrestrial Lidar, and UAV Photogrammetric

Capture Data Elevations over Different Terrain Types. Infrastructures, Vol. 5, No. 8, 2020. https://doi.org/10.3390/infrastructures5080065.

20. Yen, K. S., B. Ravani, and T. A. Lasky. LiDAR for Data Efficiency. Washington (State). Dept. of Transportation. Office of Research and Library …, 2011.

21. Haala, N., M. Peter, J. Kremer, and G. Hunter. Mobile LiDAR Mapping for 3D Point Cloud Collection in Urban Areas—A Performance Test. Int. Arch. Photogramm. Remote Sens. Spat. Inf. Sci, Vol. 37, 2008, pp. 1119–1127.

22. Habib, A., K. I. Bang, A. P. Kersting, and J. Chow. Alternative Methodologies for LiDAR System Calibration. REMOTE SENSING, Vol. 2, No. 3, 2010, pp. 874–907. https://doi.org/10.3390/rs2030874.

23. Siying, C., M. Hongchao, Z. Yinchao, Z. Liang, X. Jixian, and C. He. Boresight Calibration of Airborne LiDAR System Without Ground Control Points. IEEE GEOSCIENCE AND REMOTE SENSING LETTERS, Vol. 9, No. 1, 2012, pp. 85–89. https://doi.org/10.1109/LGRS.2011.2161070.

24. Pusztai, Z., I. Eichhardt, and L. Hajder. Accurate Calibration of Multi-LiDAR-Multi-Camera Systems. SENSORS, Vol. 18, No. 7, 2018. https://doi.org/10.3390/s18072139.

25. Barber, D., J. Mills, and S. Smith-Voysey. Geometric Validation of a Ground-Based Mobile Laser Scanning System. ISPRS JOURNAL OF PHOTOGRAMMETRY AND REMOTE SENSING, Vol. 63, No. 1, 2008, pp. 128–141. https://doi.org/10.1016/j.isprsjprs.2007.07.005.

26. Ravi, R., Y.-J. Lin, M. Elbahnasawy, T. Shamseldin, and A. Habib. Simultaneous System Calibration of a Multi-LiDAR Multicamera Mobile Mapping Platform. IEEE JOURNAL OF SELECTED TOPICS IN APPLIED EARTH OBSERVATIONS AND REMOTE SENSING, Vol. 11, No. 5, 2018, pp. 1694–1714. https://doi.org/10.1109/JSTARS.2018.2812796.

27. Glennie, C. Rigorous 3D Error Analysis of Kinematic Scanning LIDAR Systems. JOURNAL OF APPLIED GEODESY 1 (3) , pp.147-157, 2007, p. pp.147.

28. Cross, C., M. Farhadmanesh, and A. Rashidi. Assessing Close-Range Photogrammetry as an Alternative for LiDAR Technology at UDOT Divisions. Utah. Dept. of Transportation. Division of Research, 2020.

29. Luhmann, T., C. Fraser, and H.-G. Maas. Sensor Modelling and Camera Calibration for Close-Range Photogrammetry. ISPRS Journal of Photogrammetry and Remote Sensing, Vol. 115, 2016, pp. 37–46.

30. Gabrlik, P., A. la Cour-Harbo, P. Kalvodova, L. Zalud, and P. Janata. Calibration and Accuracy Assessment in a Direct Georeferencing System for UAS Photogrammetry. International journal of remote sensing, Vol. 39, No. 15–16, 2018, pp. 4931–4959.

31. Parve, L. 3D Engineered Models for Construction. Understanding the Benefits of 3D Modeling in Construction: The Wisconsin Case Study. In Rep. to Wisconsin Department of Transportation.

32. Kavanagh, B. F., and D. K. Slattery. Surveying: With Construction Applications. Pearson Upper Saddle River, NJ, USA, 2010.

33. Slattery, K. T., D. K. Slattery, and J. P. Peterson. Road Construction Earthwork Volume Calculation Using Three-Dimensional Laser Scanning. Journal of surveying engineering, Vol. 138, No. 2, 2012, pp. 96–99.

34. Schexnayder, C. J., and R. E. Mayo. Construction Management Fundamentals. McGraw-Hill Professional, 2004.

35. Slattery, K. T., and D. K. Slattery. Modeling Earth Surfaces for Highway Earthwork Computation Using Terrestrial Laser Scanning. International Journal of Construction Education and Research, Vol. 9, No. 2, 2013, pp. 132–146.

36. South Carolina Department of Transportation (SCDOT). Section 200 Earthwork: General Guidelines. 2004.

37. National Map Accuracy Standards, USGS

CHAPTER FOUR

PAPER III SAFETY ASSESSMENT OF DESIGN SPEED ON HORIZONTAL AND VERTICAL CURVES USING MOBILE LIDAR AND UNMANNED AERIAL VEHICLE PHOTOGRAMMETRY

Abstract

The process of evaluating roadway geometry for potential safety problems requires precise measurement of various geometric parameters. This study evaluated the use of mobile LiDAR scanning (MLS) point clouds and unmanned aerial vehicle (UAV) imagery-based point clouds to estimate design speeds on horizontal curves and sight distance and design speeds on vertical curves of constructed roadways. Results from paired t-test

statistical analyses at a 95% confidence level indicated that LiDAR and UAV photogrammetry systems provide horizontal curvature data at sufficient accuracy to estimate curve design speeds. The proposed methodology can be used to identify locations where the posted speed limit/advisory speed is higher than the design speed along horizontal curves so that corrective measures can be implemented on existing roadway networks. Similarly, vertical alignment data were extracted from terrain models generated from point clouds for sight distance and design speed estimation on crest and sag vertical curves. Extracted longitudinal grades were compared based on a minimum acceptable accuracy value of ± 0.5% specified by SHRP2. The statistical analysis indicated that the average deviations between field survey measurements and longitudinal grade measurements extracted from LiDAR and imagery-based point clouds were less than the acceptable accuracy value of ± 0.5% at a 95% confidence level. Additionally, the results showed that sight distances calculated using terrain models from point clouds could be used to obtain accurate estimates of design speed on vertical curves based on the results from a paired t-test statistical analysis using a 95% confidence level. Geometric characteristics of the study area, located in Anderson, South Carolina, include 4 horizontal curves and 5 vertical curves. The proposed approach offers advantages over extracting information from design drawings which may be unavailable, outdated, or inconsistent with the as-built roadway.

Keywords: Roadway Safety, Mobile LiDAR, Close-Range Photogrammetry, Roadway Geometry, as-built data, SHRP2.

Introduction

Yearly, state transportation agencies and industry practitioners strive to develop and implement proactive approaches to collect roadway data critical to enhancing maintenance efforts and address potential road safety issues to reduce the likelihood of vehicle crash occurrences. Motor vehicle crashes contribute to a significant number of injuries and fatalities in the United States and globally. Inefficient data collection methods, data availability issues, and data incompleteness complicate efforts to develop accurate road feature inventories for road maintenance and safety evaluations. Recent studies have indicated that remote sensing technologies can enhance roadway feature data acquisition and maintenance strategies (1, 2). Automated surveying practices require less field time, reduced crew sizes, and minimize human error (3).

Emerging technologies such as Light Detection and Ranging (LiDAR) and Close-Range Photogrammetry (CRP) allow for rapid and accurate collection of georeferenced three-dimensional (3D) data facilitating efforts to develop efficient data collection workflows. To date, research studies have shown that mobile LiDAR scanning (MLS) systems and CRP data collected using unmanned aerial vehicles (UAVs) have numerous applications in transportation (4). For instance, to comply with pragmatic performance measures and performance-based funding, state transportation agencies have been using innovative and practical methods and technologies to manage roadway assets (5). MLS point clouds have the potential to enhance the ability to design and maintain roadway networks by providing highly accurate, dense, and georeferenced data sets. UAV imagery-

based point clouds provide similar advantages including the ability to generate highly accurate 3D models.

Additionally, the use of innovative surveying technologies and 3D models to create virtual representations of existing roadway infrastructure provides numerous advantages including the ability to develop fast and efficient inspection protocols such as verification of compliance with design standards; and enhanced accuracy, cost-efficiency, and safety during construction and data collection activities (6). The ability to rapidly collect accurate, georeferenced, high-resolution three-dimensional data provides significant benefits over conventional surveying methods. Most conventional data collection approaches are labor intensive, time-consuming, and may expose field crews and the public to unsafe conditions. Conventional survey data are collected at sample locations and are not continuous. Thus, locations between surveyed points are interpolated which may compromise overall accuracy. Additionally, design drawing data of existing roadways may be inconsistent with the as-built roadway. That is, as-built measurements are often not available and design drawing data may not be accurate because the as-built roadway may not correspond with preconstruction design drawings (7). This issue is particularly prevalent when older roadways are considered.

From a safety standpoint, identifying locations where vehicles may exceed design speeds is critical in preventing future crashes. A proactive approach that identifies potential design deficiencies is favorable to analyzing crash data.

This study evaluates the feasibility of MLS and imagery-based point clouds collected by CRP UAVs to extract horizontal and vertical roadway geometry features for

design speed and sight distance assessment on constructed roadways. Comparisons were made using geometric elements extracted from MLS data collected by five vendors, and aerial imagery and manual survey data collected by the research team.

LITERATURE REVIEW

Applications of MLS in transportation

LiDAR systems can be used to acquire large data sets of high-accuracy three-dimensional (3D) point clouds in a timely manner. Additional benefits include less personnel exposure to potentially hazardous conditions during data collection activities and fewer unnecessary delays for the traveling public when compared to some conventional survey methods (1). The Federal Highway Administration (FHWA) has identified LiDAR as a technology that could help consolidate resources, maximize funding, and enhance the accuracy and integration of information (2). LiDAR data sets can be obtained in a variety of ways using static, mobile, and aerial systems. These systems are ideal for rapid and safe data collection; thus, enhancing the ability to complete tasks more efficiently and in a safer environment. Moreover, mobile LiDAR systems have become an effective solution for rapid data collection given developments in scanning speed and accuracy, global positioning systems (GPS), and inertial measurement units (IMU) (3). Attempts to extract roadway features are discussed in the following paragraphs.

A review of literature shows numerous fully automated and semi-automated 2D and 3D approaches to extract lane markings from LiDAR point clouds. For example,

(Ogawa and Takagi, 2006) attempted to extract lane markings using two-dimensional (2D) scanning LiDAR. In their study, lane curvature was calculated using Hough transformation, and lane widths were calculated using a statistical procedure. Their algorithm offered promising results and was based solely on LiDAR range data (4).

The importance of lane markings as a pre-requisite for many driver assistance systems and autonomous vehicles was highlighted in a study by Kammel and Pitzer (5) who proposed an algorithm to not only detect lane markings but also enable the creation of topological maps of the traversed street sections. Similarly, Lindner et al. (6) proposed a method to extract lane markings from LiDAR data based on reflectivity and distance information. Cheng et al. suggested two approaches for lane marking extraction from LiDAR point clouds based on intensity thresholds and deep learning (7). Several other studies have used mobile LiDAR data to detect and extract road pavement markings (8–11), and to estimate and evaluate pavement marking reflectivity (12).

Lin and Hyyppa (13) proposed a multistep automated approach to detect culverts in MLS point clouds. The authors reported measurement errors between 9% and 16%. A study by Landa and Prochazka (14) compared road information that can be obtained from RGB images and LiDAR measurements. Their study focused on road signs, road markings, and pole-shaped objects including light poles and trees.

A framework for extracting road and roadside information using remote sensing data obtained from multiple sources was proposed by Ural et al. (15) The study showed that 90.25% of a total of 23.6 miles of road networks, and 90.6% of 107 existing buildings were correctly identified and extracted using orthophotos and airborne LiDAR point

clouds. Additionally, the authors estimated average grades, cross-section lines, and cross-slopes based on identified road centerlines and roadside areas.

Guan at al., (16) conducted a review of the literature to identify advancements in mobile LiDAR technology and their applications in road information inventory. The study reviewed aspects related to system components, direct georeferencing, data error analysis, geometrical accuracy validation, and extraction of road surfaces and pole-like objects. In their review, the authors pointed out the importance of accuracy verification, primarily because mobile LiDAR systems have certain limitations and perform differently based on factors such as range, incidence angle of laser pulse to the reflective object, and accuracy of GPS and IMU.

Gouda et al. (17) attempted to map and assess roadside clearance parameters using mobile LiDAR on rural highways. The authors employed a voxel-based ray-casting approach for collecting inventories of roadside assets and for mapping and assessing roadside clearance parameters. The study mentions that the proposed method was tested on four highway segments with edge detection accuracies ranging from 97% to 98.5%.

An earlier study by Findley et al. (18) compared roadway data collected using manual methods to data collected by manned data collection vehicles moving with traffic. The authors compared various roadway elements including curbs, guardrails, signs, pavement markings, and roadway geometry.

Gargoum et al, (19) attempted to used LiDAR data to automatically evaluate sight distance along a two-lane undivided rural highway. The authors defined observer and target points along travel lanes based on a surface terrain model. Their methodology was based

on a two-step process that uses ArcGIS tools for distance assessment and a Microsoft VB algorithm for processing and analyzing the outputs attained from GIS. The authors constructed lines of sight based on pairs of points identified as target and observer and used a VB code to estimate the sight distance available to each observer. Their results showed that minimum stopping sight distance (SSD) requirements were violated on a portion of the analyzed highways. Specifying the number of observer points at which testing is required and the trade-off between the number of points and processing time were identified as limitations associated with their methodology. The authors verified the results by comparing obstructed sight lines using images from the field at obstructed locations. Another study by Gargoum and El-Basyouny (20) performed a review of studies that proposed approaches to extract information from LiDAR data for transportation applications. The authors argued that few studies have attempted to extract roadway design elements from LiDAR data sets and highlighted areas where research might be needed.

(Ma et al., (21) proposed a procedure for visualizing sight distance along an existing roadway in real-time using MATLAB and LiDAR data. The method uses LiDAR data for 3D sight distance estimation in highway environments with complex roadside obstacles. The authors compared their results with sight distance data obtained using digital terrain models and ArcGIS tools.

In a recent study, Salkamy et al., (22) proposed a fully automated algorithm for large-scale assessment of available sight distance in a three-dimensional space using LiDAR. The authors looked at historical collision data along sections identified has having insufficient sight distance and concluded that sight distance limitations could have

contributed to collision occurrences. Similarly, Agina et al., (23) proposed a procedure to assess passing sight distance on two-lane highways using mobile lidar. Their method involved extracting centerline lane markings, defining passing-allowed and passing-prohibited regions, followed by computations of sight distance. Their study found roadway sections where passing was not allowed but there was adequate sight distance for passing maneuvers and sections with insufficient sight distance where passing was allowed.

Photogrammetry Applications in Transportation

Although LiDAR technology and its applications in transportation have gained increasing popularity in recent years, researchers and practitioners have attempted to accomplish similar results using reliable and cost-effective alternatives to LiDAR such CRP. Photogrammetric approaches offer a less expensive, user-friendly alternative to LiDAR technologies (24). Cross et al. suggests that LiDAR creates more uniform and accurate point clouds, but photogrammetry generates similar high-quality point clouds that are also highly accurate. Their study suggests that photogrammetry is a cost-effective technology that can be used to achieve similar results to LiDAR.

Bassani et al. (25) attempted to use a point cloud from images collected along a roadway segment to perform sight distance analysis using ArcGIS tools. The authors created a terrain model from the point cloud which was analyzed in the ArcGIS environment.

A study by Farhadmanesh et al. explored the possibility of using photogrammetry as an alternative to LiDAR for highway asset and pavement condition assessment. The

authors identified instances where some of their models generated using photogrammetry were denser than models generated using LiDAR; though typically LiDAR point cloud models tend to be denser than those created using photogrammetry (26).

Three-dimensional (3D) models based on 2D images reconstructed from UAV photogrammetry were used in a study by Nappo et al. (27) to develop an objective and less laborious alternative to traditional field surveys for semi-automatic damage assessment of asphalt-paved roads in landslide affected areas. Their study used 3D models and 2D images reconstructed from UAV-based photogrammetry to detect longitudinal and transverse cracks on the road pavement and assess their severity in landslide areas.

Summary of Previous Studies

While the literature identified a number of studies that extracted horizontal and vertical road geometry, and sight distance information from LiDAR point clouds, few studies compared results from data collected using multiple data collection systems. In addition, it is worth noting that to our knowledge, many studies did not validate their results using ground truth data from field surveyed measurements. This research expands on previous studies by comparing geometry data extracted from multiple mobile LiDAR sources and evaluates the MLS accuracy by comparing the results from manual survey measurements. Additionally, this research evaluates the extraction of highway alignment data from CRP imagery-based point clouds from high-resolution UAV images and directly compares the results to the MLS and manual survey measurements. No other study could be identified in the literature that performed a similar comparison.

OVERVIEW OF STUDY AREA

The study was conducted along a 1.3-mile section of a 4-lane mostly divided parkway located in Anderson, South Carolina. This roadway is classified as an urban principal arterial with a factored Annual Average Daily Traffic (AADT) of approximately 13700 vehicles per day. Geometric characteristics of the roadway section include four vertical curves, five vertical curves and two lanes in each direction. Figure 4-1. shows a panoramic photograph of a short section and an aerial image of the entire study area.

Figure 4-1 Stations and GCP locations along the study area.

DATA COLLECTION AND PROCESSING

Manual Data Collection

The research team, which included a professional land surveying crew, manually surveyed the entire 1.3-mile roadway segment to locate 100-foot stations along the pavement edge lines. 424 points were manually collected on the edge lines of the roadway and across each station where lane markings were present. In total, the study area consisted of sixty-nine 100-foot survey stations established on both sides of the roadway along the edge lines. In addition, a ground control survey was conducted to locate primary ground control points (GCPs) consisting of existing geodetic survey markers, and secondary GCPs established by the research team throughout the study area (see Fig. 4-2). Equipment used during the conventional data collection process include total stations, automatic levels, and high-accuracy GPS.

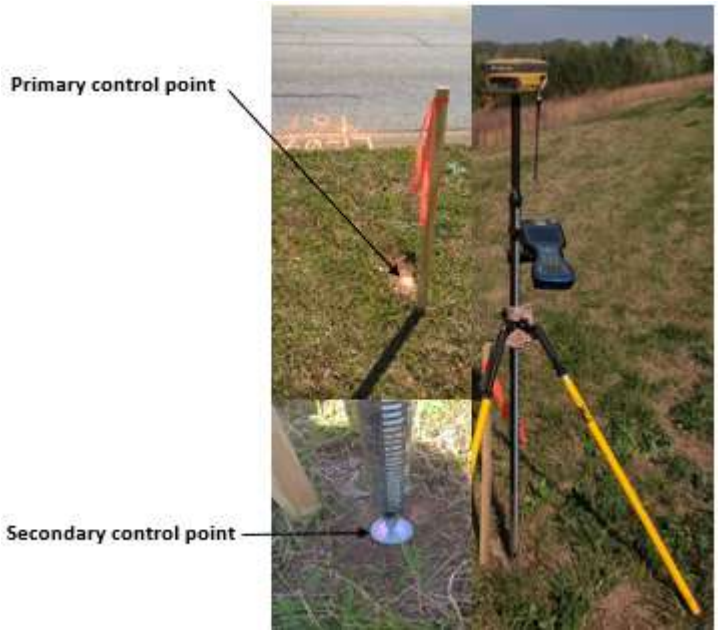

Figure 4-2 Sample primary and secondary GCPs established using high accuracy GPS.

Mobile LiDAR Data Collection

Mobile LiDAR data were collected by five participating vendors using their own equipment. Components of the MLS systems used by vendors include vehicle mounted GPS units, LiDAR sensors, IMUs, and a distance measuring instruments (DMIs). Vendors used a minimum of two primary GCPs as base station locations for GPS differential correction. All primary and secondary GCPs were used for post-processing adjustment of the LiDAR point clouds. Vendors were responsible for calibrating their respective LiDAR systems before and during the data collection process. Table 4-1 provides a summary of the MLS equipment used by vendors. Vendors collected point cloud data from the right (outer) lane using one pass in each direction. Studies have shown that accurate mobile LiDAR data can be collected using one pass from either lane on multilane highways (28). A LiDAR point cloud collected by a vendor is shown in Figure 4-3. Survey stations were marked with PK surveying nails. In addition, the research team used reflective pavement marking tape to ensure that PK nail locations could be easily identified in LiDAR and UAV photogrammetry-based point clouds using the intensity and RGB color attributes, respectively (See Fig 4-3).

Table 4-1 Mobile LiDAR Equipment Specifications

Equipment Specifications		Mobile LiDAR systems				
		Vendor A	Vendor B	Vendor C	vendor D	Vendor E
LiDAR	Brand Name	Riegl	Teledyne Optech	Optech	Z+F Profiler	Optech
	Model	VMX450	SG1	M1	9012	M1
	Laser	Dual	Dual	Dual	Single	Dual
	Measurement rate	1100 KHz	600 KHz/sensor	500 KHz/sensor	1000 KHz	500 KHz/sensor

DMI	Brand	APPLANIX	Applanix	Applanix	N/A	Applanix
	Model	BEI HH5	HS35F	LV	N/A	LV
IMU	Brand	APPLANIX	N/A	Northrop Grumman	NovAtel	Northrop Grumman
	Model	ap50	FMU P301	LN 200	SPAN IMU-FSAS	LN 200
	Roll/pitch accuracy	0.005°	0.005°	0.25°	0.008°	0.25°
	Heading Accuracy	0.015°	0.015°	0.50°	0.013°	0.50°
Camera	Type	NIKON/RIEGL	Point Grey 360°	Optech	Leica	Optech
	Number of cameras	2Front/2Rear 4 TOTAL	6 total spherical array	2Front/2Rear 4 TOTAL	7 total spherical array	2Front/2Rear 4 TOTAL
	Frame rate	15 fps	3 fps	2 fps	8 fps	3 fps
	Resolution	5 MP	5 MP	5 MP	4 MP	5 MP
GPS/GNSS	Brand	TRIMBLE	Trimble	Trimble	NovAtel	N/A
	Model	Zepher model 2	AT1675-540TS	Zephyr model 2	GPS-702-GG	N/A
	Accuracy	10 mm	0.02’ H; 0.04’ V	Survey Grade	N/A	N/A

N/A: Not available (Specification not provided by vendor)

Figure 4-3 Sample LiDAR point cloud and reflective marking tape used to identify stations established along the edge of pavement (EOP) lines.

Unmanned Aerial Vehicle (UAV) Imagery Data Collection

Low-altitude UAV photogrammetry data were collected using a commercially available UAV (Phantom 4 Pro) with a 20MP imager (See Figure 4a). Two altitudes were

used to collected UAV imagery data: 117 ft above ground level (AGL), and 288 ft AGL from point of takeoff, respectively. Aerial targets were used to facilitate the identification of primary and secondary GCPs (see Figure 4b). In this study, the imagery-based point cloud was adjusted using four GCPs.

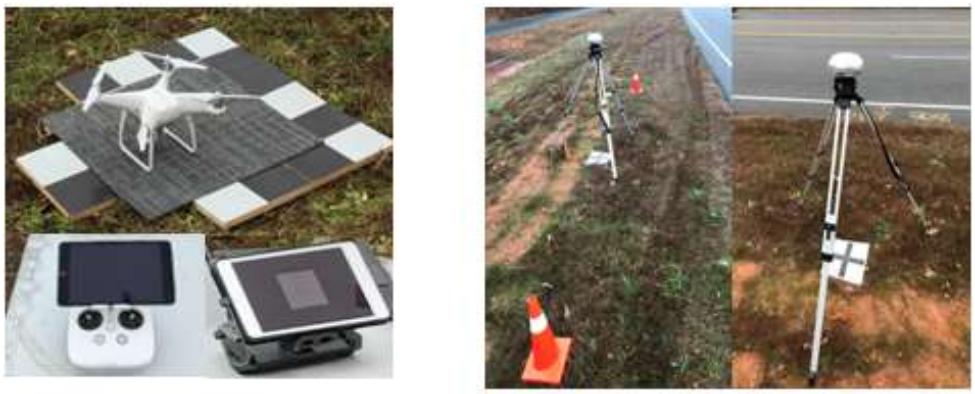

(a) UAV system (b) Aerial targets

Figure 4-4 Unmanned aerial vehicle (UAV) system and targets used during low-altitude imagery data collection.

DATA ANALYSIS AND RESULTS

Comparison of Horizontal Curvature Data

Ground truth horizontal alignment data were manually collected relative to the centerline of the roadway using state-of-the-art surveying equipment. Comparisons were made using horizontal alignment data extracted from point clouds relative to the centerline of the roadway (See figure 4-5). Reference survey stations located along the edge lines and lane markings identifiable using the intensity attribute of LiDAR point clouds, and RGB color attributes of the imagery-based point cloud were used to extract tangent lines and

horizontal curvature data in a semi-automated fashion using OpenRoads Designer design software.

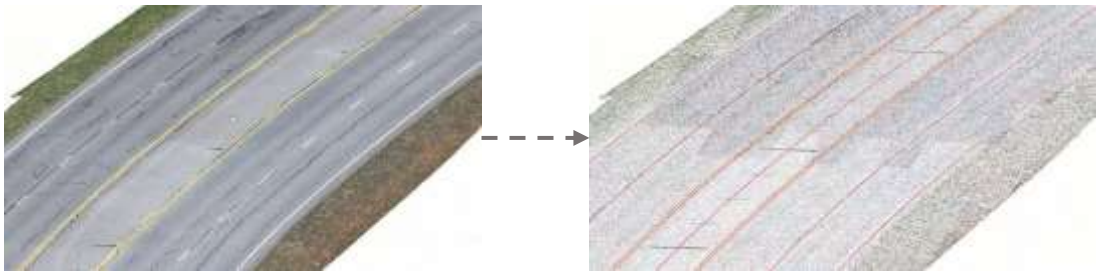

Figure 4-5 Extraction of road centerline from point cloud data.

A comparison of ground truth horizontal alignment data collected using traditional surveying methods, and horizontal alignment data derived from LiDAR and UAV imagery-based point clouds is presented below (See Table 4-2). The data included in this comparison represent the most common horizontal curve parameters used in roadway design.

Table 4-2 Comparison of Manually Surveyed Data and Horizontal Alignment Data Extracted from Point Clouds.

Horizontal Curve #	Horizontal Curve Parameter	Field Survey Data (ft) (Ground Truth)	Deviations of extracted values from field survey data (ft)					
			Mobile LiDAR point clouds (Vendors)					Imagery-based point cloud
			A	B	C	D	E	
Curve 1	PC	153+61.78	+12.21	+7.09	-2.85	-8.48	+1.39	+11.89
	PI	166+51.26	-0.04	-1.36	-3.80	-6.96	-2.74	+3.53
	PT	177+10.88	-7.52	-6.44	-4.35	-5.63	-4.98	-1.46
	R	2291.83	-6.51	-3.99	-0.37	+3.18	-0.51	-3.74
	L	2349.10	-19.74	-13.53	-1.50	+2.84	-6.37	-13.35
	T	1289.47	-12.25	-8.45	-0.95	+1.52	-4.13	-8.36
	M	294.45	-4.03	-1.90	-0.32	+0.31	-1.65	-2.81
Curve 2	PC	182+37.69	+6.97	+10.59	+12.32	+14.74	+13.73	-1.16
	PI	187+69.77	+9.07	+9.14	+7.71	+8.51	+7.16	-6.76

	PT	192+89.87	+11.11	+7.79	+3.30	+2.54	+0.84	-11.96
	R	2864.79	+9.19	+1.20	-13.19	-19.24	-21.84	+5.10
	L	1052.17	+4.14	-2.80	-9.01	-12.20	-12.90	-10.80
	T	532.08	+2.10	-1.46	-4.60	-6.23	-6.58	-5.61
	M	48.17	+0.23	-0.27	-0.60	-0.79	-0.81	-1.07
Curve 3	PC	199+96.63	-4.12	-0.57	-3.48	-5.01	-4.62	+25.84
	PI	203+49.89	-24.32	-1.24	-0.72	-1.59	-0.87	+17.09
	PT	206+95.28	-43.86	-1.93	+1.96	+1.72	+2.77	+8.60
	R	1909.86	-81.02	-7.14	+12.09	+14.11	+17.02	-40.04
	L	698.65	-39.75	-1.36	+5.44	+6.74	+7.40	-17.25
	T	353.27	-20.21	-0.67	+2.76	+3.43	+3.75	-8.75
	M	31.86	-2.26	-0.00	+0.29	+0.38	+0.39	-0.90
Curve 4	PC	212+39.79	+20.46	-1.12	-1.17	-2.55	-2.83	-12.26
	PI	218+24.45	+5.34	+3.31	+3.63	+2.28	+3.47	+5.04
	PT	223+84.68	-8.32	+7.49	+8.09	+6.77	+9.31	+20.82
	R	2291.83	-17.92	+14.81	+12.00	+12.51	+15.37	+29.62
	L	1144.89	-28.77	+8.61	+9.27	+9.32	+12.14	+33.08
	T	584.65	-15.11	+4.42	+4.80	+4.83	+6.30	+17.30
	M	71.12	-2.99	-0.21	+0.78	+0.77	+0.84	+3.20

Mean percentage absolute errors (MAPE) and the expected accuracy (100-MAPE) of extracted measurements were calculated using equation (4-1). Results for all the measurements are shown in table 4-3.

$$MAPE = \frac{1}{n}\sum_{t=1}^{n} \left| \frac{A_t - F_t}{A_t} \right| \qquad (4\text{-}1)$$

Where n is the number of data points (n=20 data points per parameter from LiDAR point clouds; n=4 data points per parameter from the imagery-based point cloud), A_t is the actual value represented by the surveyed ground truth data, and F_t is the extracted value from the MLS data.

Table 4-3 Summary of Horizontal Alignment Measurement Comparisons

Summary		PC	PI	PT	R	L	T	M
Mobile LiDAR Point Clouds	MAPE (%)	0.037	0.027	1.675	0.647	1.020	1.042	1.335
	100-MAPE (%)	99.96	99.97	98.32	99.35	98.98	98.96	98.66
Imagery-based Point Cloud	MAPE (%)	0.068	0.041	0.051	0.933	1.738	1.785	2.624
	100-MAPE (%)	99.93	99.96	99.95	99.07	98.26	98.22	97.38

Overall, the research team was able to extract desired data elements with reliable levels of accuracy that were within or below the target accuracies specified by SHRP2 (see table 4-2). For instance, SHRP2 recommends a point of curvature (PC) accuracy of ±3 ft. However, the best achieved accuracy by SHRP2 was -154.97 ft. In this study, the best achieved PC accuracy from LiDAR data was -0.567 and the worst PC accuracy was +20.456 ft. This indicates that the best accuracy achieved in this study using LiDAR data was less than the maximum acceptable deviation recommended by SHRP2. Additionally, SHRP2 recommends a horizontal curve length accuracy of ±2 ft and a curve radius accuracy of ± 25 ft. In this study, the best achieved accuracies for curves length and curve radius extracted from LiDAR data were -1.360 ft and -0.367 ft, respectively. The worst achieved accuracies for curve length and curve radius extracted from LiDAR data were -39.745 ft and -81.0.25 ft respectively.

Similarly, the best achieved accuracy for PC data extracted from the imagery-based point cloud was -1.156 ft and the worst PC accuracy was +25.844 ft. The best achieved accuracies for horizontal curve length and curve radius extracted from the imagery-based point cloud — best (worst) — were as follows: curve length -10.804 ft (+33.082), and curve radius -3.739 ft (-40.041 ft). Therefore, most of the horizontal curve parameters extracted from the imagery-based point cloud were within the recommended accuracy

values specified by SHRP2 except for the curve length data which were all above the recommended accuracy value, and the curve radii data which varied the most. Overall, these results indicate that LiDAR point clouds are a relatively more reliable source of accurate horizontal curvature data compared to UAV imagery-based point clouds.

Extraction of Maximum Superelevation Rate (e_{max}) from Point Clouds

Superelevation is commonly defined as the banking of a roadway along horizontal curves to assist drivers in resisting the effect of centrifugal force, allowing them to navigate horizontal curves safely at reasonable speeds. While the selection of a maximum rate of superelevation depends on several factors, the SCDOT specifies a maximum superelevation rate of 8% for all facilities with design speeds between 50 mph and 75 mph (29). Table 4-4 shows potential adverse impacts to safety if as-built superelevation deviates from specified design criteria.

Table 4-4 Potential Adverse Safety Impacts of Deviation from Design Criteria (30).

Safety & Operational Issues	Freeway	Expressway	Rural Two-Lane	Urban Arterial
Run-off-road crashes	X	X	X	
Cross-median crashes	X	X		
Cross-centerline crashes			X	
Skidding	X	X	X	X
Large vehicle rollover crashes	X	X	X	

Note: Freeway: high-speed, multi-lane divided highway with interchange access only (rural or urban); Expressway: high-speed, multi-lane divided arterial with interchange and at-grade access (rural or urban); Rural 2-Lane: high-speed, undivided rural highway (arterial, collector, or local); Urban Arterial: urban arterials with speeds 45 mi/h (70 km/h) or less.

A multistep approach was used to extract maximum superelevation rate values on horizontal curves using point cloud data as follows: a) Identification of mid-point of curve using extracted horizontal curvature parameters. b) Delineation of perpendicular buffer area relative to the mid-point of the curve, c) Extract elevations and calculated distances of LiDAR points along the superelevated cross section using a surface model, d) perform linear regression on the extracted LiDAR points to determine the cross slope which represents the maximum superelevation rate. Figure 4-6 and Figure 4-7 illustrate the process of extracting maximum superelevation data from point clouds.

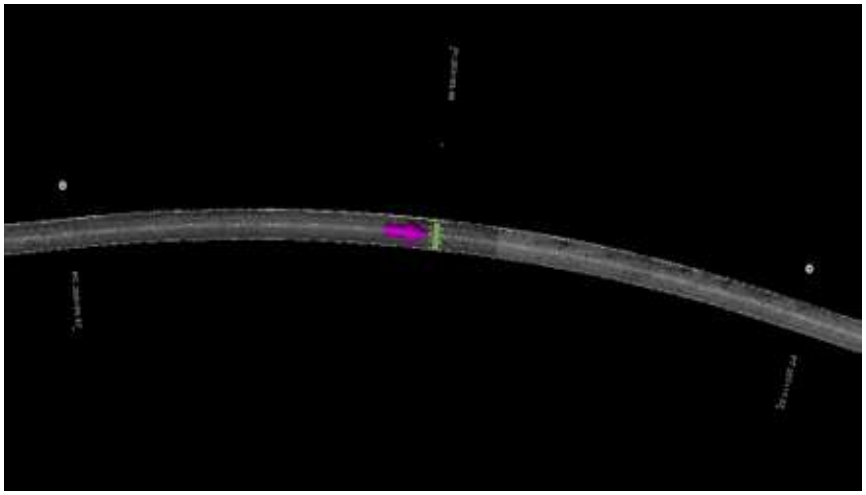

Figure 4-6 LiDAR point cloud of a horizontal curve: Vendor C (curve 1)

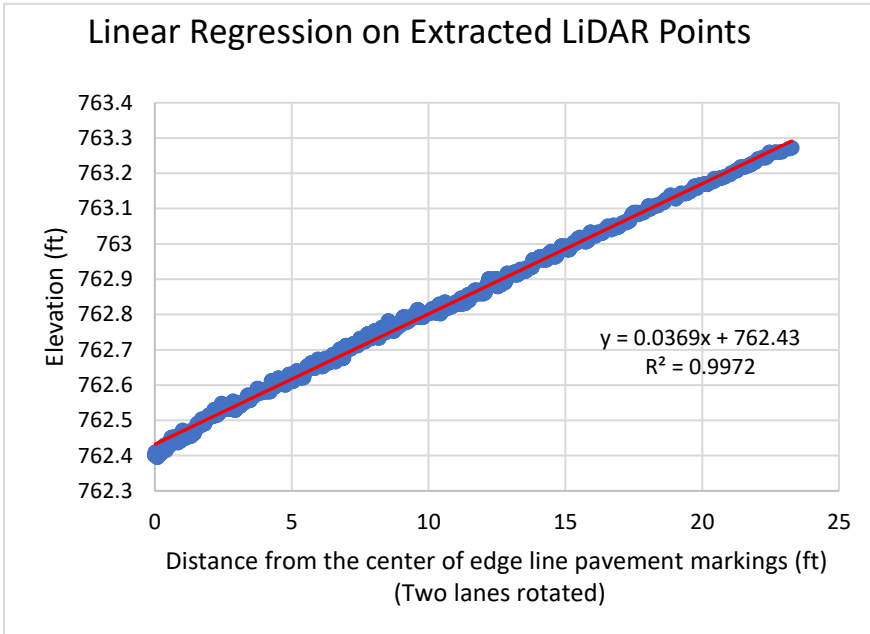

Figure 4-7 Extraction of maximum superelevation rate from point cloud: Vendor C (curve 1)

Design Speed Estimation on Horizontal Curves

In accordance with AASHTO recommendations, the radius used to estimate the design speed on horizontal curves was measured to the inside edge of the innermost travel lane. This is done to consider the motorist operating within the innermost travel lane, particularly for multilane roadways with sharp horizontal curves (31). Per the AASHTO green book, horizontal curve equations do not consider the width of the roadway. Equation (4-2) describes the relationship between curve radius and design speed. Design speed can be solved for by substituting values for R, e, and f.

$$R = \frac{v^2}{15\,(e+f)} \tag{4-2}$$

Where:

R = Radius of curve

V= Design speed
e = Design superelevation rate
f = Design friction coefficient

Horizontal curve geometry parameters can be estimated using existing maps, high resolution Google Earth images, UAV images, point clouds, and GPS trajectories. However, superelevation data cannot be obtained from 2D data sets. Design speed estimates from 2D data require the use of an assumed design superelevation rate or field measurements using specialized devices (ball-bank indicator, inertial device, etc.). High-accuracy 3D point clouds provide both 2D and 3D data that can be used to collect both radii and superelevation data. Therefore, this study used 3D point clouds to estimate design speeds on horizontal curves.

An alternative method not requiring site visits was also used to extract horizontal geometry data for comparison purposes. This was done using Google Earth images. To manually estimate design speed from radii data extracted from Google Earth Pro images, chord length (C) and middle ordinate distance (M) were measured in Google Earth relative to the inside edge of the innermost travel lane in the direction of travel (see figure 4-8). Using equation (4-3, 4-4) the radius can be estimated; however, superelevation must be assumed. The actual long chord from the PC to the PT of a curve is not needed to estimate the radius. This is important because it is difficult to identify the exact locations of the PC and PT just from imagery data. Only a chord that is clearly on the curve is needed. The design speeds for curve radius data extracted manually from google earth images are shown in table 4-5. The calculated design speeds used superelevation rates from manual field measurements for consistent comparison.

$$R^2 = (R - M)^2 + (\frac{C}{2})^2 \quad (4\text{-}3)$$

$$R = \frac{1}{2}M + \frac{C^2}{8M} \quad (4\text{-}4)$$

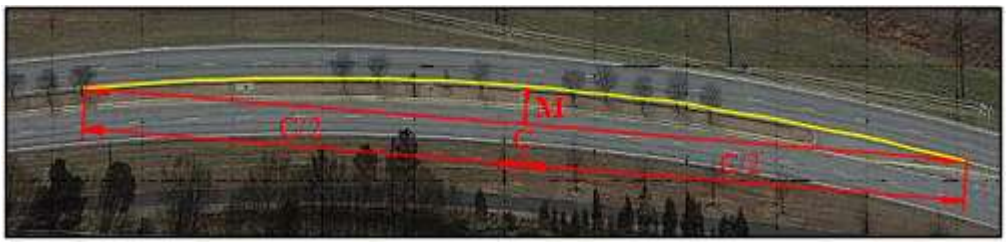

Figure 4-8 Middle ordinate distance (M) and Chord length (C) measured relative to the inside edge of the innermost travel lane in Google Earth Pro.

Radii data from all sources extracted relative to the inside edge of the innermost travel lane are shown in Table 4-5. In addition, Table 4-5 shows extracted maximum superelevation rate data as well as estimated design speeds based on equation (2).

Table 4-5 Horizontal Curve Design Speed Estimation based on Extracted Horizontal Curvature and Superelevation Data

Parameter	Source of Data		Eastbound (EB) Travel Lanes				Westbound (WB) Travel Lanes			
			HC 1	HC 2	HC 3	HC 4	HC 1	HC 2	HC 3	HC 4
Radius (ft) Edge of Innermost Travel Lane	Manual Survey		2260.8	2871.9	1878.6	2322.9	2298.9	2833.5	1917.4	2260.6
	Mobile LiDAR Vendors	A	2254.2	2881.6	1797.8	2281.7	2293.2	2842.9	1836.6	2242.7
		B	2256.5	2873.7	1871.6	2314.5	2295.5	2834.9	1910.3	2275.4
		C	2275.4	2859.3	1890.9	2311.7	2299.3	2820.6	1929.8	2272.6
		D	2263.7	2853.3	1892.9	2312.2	2302.8	2814.5	1931.7	2273.1
		E	2260.2	2850.6	1895.9	2315.1	2299.2	2811.9	1934.7	2275.9
	UAV-CRP		2256.9	2877.6	1838.9	2329.3	2295.9	2838.8	1877.5	2290.2
	Google Earth Imagery		2255.8	2808.6	1848.2	2291.5	2287.6	2804.5	1908.4	2238.4
	Manual Survey		3.74%	2.79%	3.96%	2.42%	3.61%	2.86%	3.91%	3.76%

Extracted e max (%)	Mobile LiDAR Vendors	A	3.61%	3.06%	4.00%	2.72%	3.61%	2.89%	3.80%	3.90%
		B	3.67%	3.10%	4.05%	2.68%	3.67%	2.80%	3.97%	3.85%
		C	3.69%	3.04%	3.98%	2.70%	3.67%	2.83%	4.02%	3.85%
		D	3.65%	3.07%	4.03%	2.66%	3.60%	2.85%	3.96%	3.84%
		E	3.85%	2.88%	4.11%	2.47%	3.68%	2.78%	3.85%	3.87%
	UAV-CRP		3.39%	3.32%	4.07%	2.68%	3.51%	3.08%	3.83%	3.85%
	Google Earth Imagery		n/a	n/a	n/a	n/a	n/a	n/a	n/a	n/a
Estimated Design Speed (mph)	Manual Survey		67.1	69.2	63.7	64.1	67.1	69.2	64.0	67.1
	Mobile LiDAR Vendors	A	66.7	70.1	62.8	64.6	67.0	69.3	62.8	67.3
		B	66.8	70.3	63.8	65.0	67.2	69.0	64.0	67.5
		C	67.1	69.9	63.8	64.8	67.2	69.0	64.4	67.4
		D	66.9	69.9	64.0	64.7	67.1	69.0	64.2	67.4
		E	67.3	69.3	64.2	64.2	67.3	68.8	64.0	67.5
	UAV-CRP		66.1	70.9	63.5	64.9	66.8	69.9	63.4	67.6
	Google Earth Imagery		65.1	69.4	61.2	65.4	65.4	69.4	61.8	65.0

HC: Horizontal Curve; n/a: Not available.

Summary statistics of the superelevation rate and design speed data extracted from LiDAR point clouds provided by all vendors is shown in Table 4-6. The minimum and maximum observed standard deviations for extracted maximum superelevation rates were 0.02 and 0.1, respectively. Similarly, the minimum and maximum standard deviations for calculated design speeds were 0.09 and 0.61, respectively.

To compare the differences between the means of design speed data calculated using geometric features from manual survey data to design speed data calculated using geometric features extracted from point clouds, a statistical analysis was performed using

paired sample t-tests. The results of the statistical analysis shown in Table 4-6 indicate that the magnitude of the difference between the means of measurements from manual survey data and point clouds are not statistically different at a 95% confidence level. This indicates that there is a non-significant, very small difference between the means of measurements from manual survey data and measurements extracted using point clouds. Further, these results show that point cloud data can be used to obtain reliable design speed and maximum superelevation data.

Table 4-6 Summary of Superelevation and Design Speed Data Extracted from MLS Point Clouds

Data		Eastbound				Westbound			
		HC 1	HC 2	HC 3	HC 4	HC 1	HC 2	HC 3	HC 4
	Manual Survey	3.74%	2.79%	3.96%	2.42%	3.61%	2.86%	3.91%	3.76%
Superelevation (LiDAR point clouds)	Min	3.61%	2.88%	3.98%	2.47%	3.60%	2.78%	3.80%	3.84%
	Max	3.85%	3.10%	4.11%	2.72%	3.68%	2.89%	4.02%	3.90%
	Mean	3.69%	3.03%	4.03%	2.65%	3.65%	2.83%	3.92%	3.86%
	Median	3.67%	3.06%	4.03%	2.68%	3.67%	2.83%	3.96%	3.85%
	SD	0.09%	0.09%	0.05%	0.10%	0.04%	0.04%	0.09%	0.02%
		Paired t-test $H_a: \mu_d \neq 0$		P-value = 0.17 t_{obs} = 1.82 df = 3		Paired t-test $H_a: \mu_d \neq 0$		P-value = 0.37 t_{obs} = 1.06 df = 3	
	Manual Survey	67.1	69.2	63.7	64.1	67.1	69.2	64.0	67.1
Design Speed (LiDAR point clouds)	Min	66.7	69.3	62.8	64.2	67.0	68.8	62.8	67.3
	Max	67.3	70.3	64.2	65.0	67.3	69.3	64.4	67.5
	Mean	67.0	69.9	63.7	64.7	67.2	69.0	63.9	67.4
	Median	66.9	69.9	63.8	64.7	67.2	69.0	64.0	67.4
	SD	0.25	0.36	0.53	0.28	0.10	0.19	0.61	0.09
		Paired t-test $H_a: \mu_d \neq 0$		P-value = 0.24 t_{obs} = 1.47 df = 3		Paired t-test $H_a: \mu_d \neq 0$		P-value = 0.84 t_{obs} = 0.23 df = 3	

HC: Horizontal curve; SD: Standard deviation

Measurements extracted from Google Earth images were used to perform a sensitivity analysis based on different superelevation rate values (see figure 4-9 and figure 4-10). Thus, in the eastbound direction, design speed differences for superelevation rates between 2% and 8% range from about 2.5 mph to 14.6 mph for a curve radius of 2255.8 ft; 2.9 mph to 16.9 mph for a curve radius of 2808.6 ft; 2.2 mph to 12.7 mph for a curve radius of 1848.19 ft; and 2.48 mph to 14.7 mph for a curve radius of 2291.46 ft. Likewise, in the westbound direction, design speed differences for superelevation rates between 2% and 8% range from about 2.5 mph to 14.7 mph for a curve radius of 2287.6 ft; 2.9 mph to 16.9 mph for a curve radius of 2804.5 ft; 2.2 mph to 13 mph for a curve radius of 1908.39; and 2.4 mph to 14.5 mph for a curve radius of 2238.35 ft. The variation in design speed due to different superelevation rates indicates the importance of using accurate superelevation data to accurately estimate design speed.

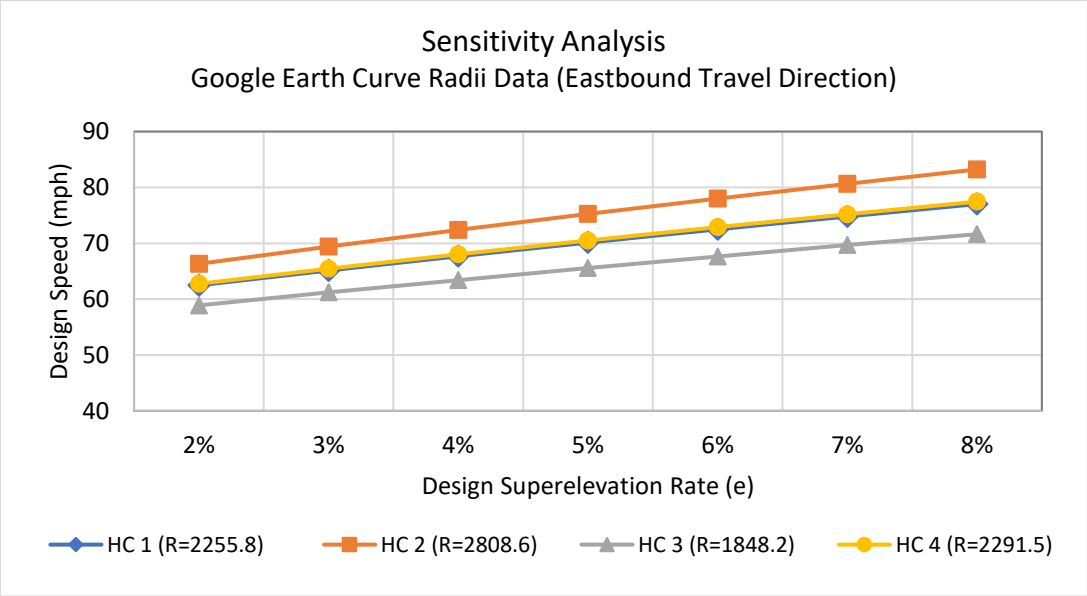

Figure 4-9 Design speed sensitivity analysis based on superelevation rate (EB)

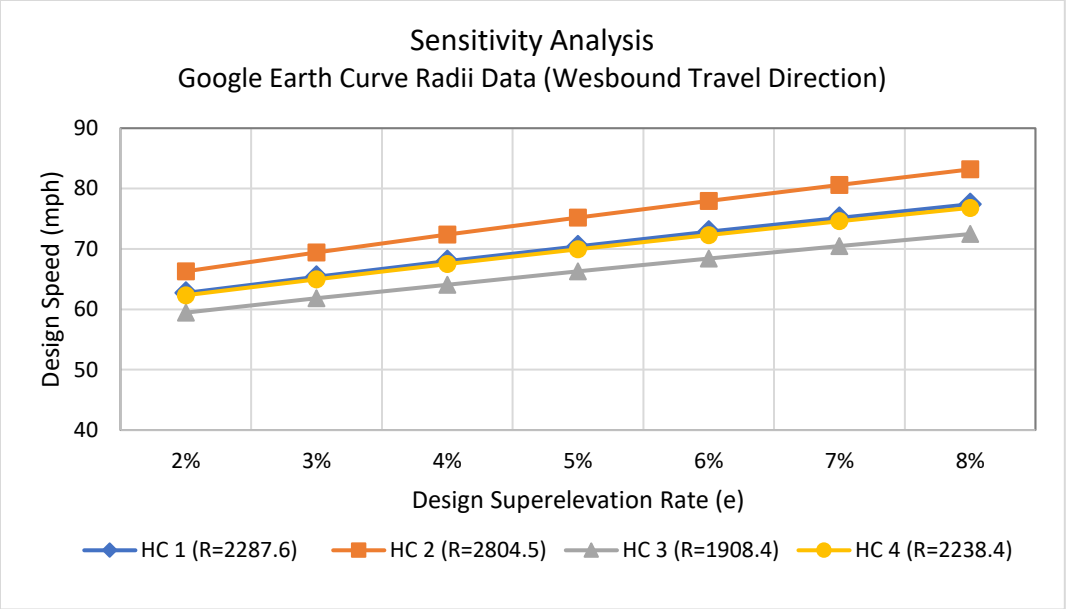

Figure 4-10 Design speed sensitivity analysis based on superelevation rate (WB)

Road Grade Estimation Using Point Clouds

Manual approaches for direct on-road measurement of road grades using equipment such as smart digital levels are time consuming and may interfere with traffic and exposes surveying crews to potentially hazardous conditions. Previous studies have shown that LiDAR data can be used to accurately estimate road grades using regression techniques (32, 33). In this study, road grades were estimated from point cloud data using linear regression on points extracted along the centerline of the roadway. Thus, grades were estimated directionally using points along the centerline of the roadway in the direction of travel (see figure 4-11). The steps can be summarized as follows: a) Select LiDAR data within a defined buffer zone. For this four-lane, mostly divided roadway, two lanes in each direction were included in the buffer zone of LiDAR points. b) Define the centerline of the roadway based on identifiable lane markings and manually surveyed reference stations; c)

segment the roadway using 100-foot segments along tangent sections based on a defined origin such that segments adequately capture changes in the road grade for consistent comparison, d) extract points along the centerline using a LiDAR surface model, e) perform linear regression on extracted LiDAR points to estimate the road grade (see figure 4-12).

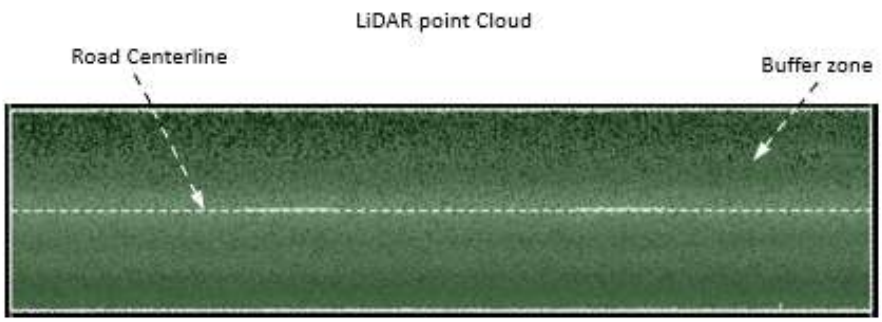

Figure 4-11 Selection of segment of lidar points for analysis.

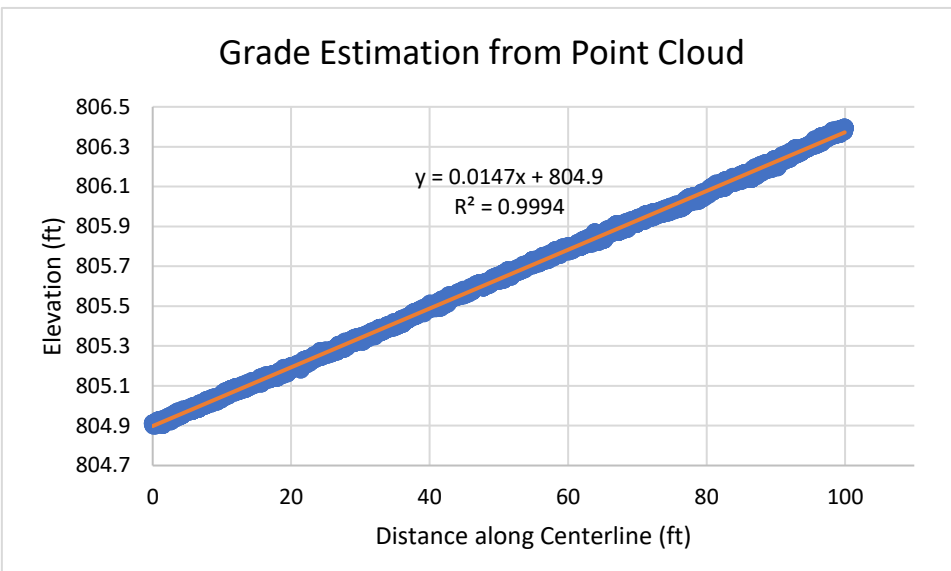

Figure 4-12 Sample grade estimation from extracted LiDAR points: Vendor C (EB).

Statistical analyses using one-sided t-tests were performed to determine if measurements extracted from point clouds were less than the minimum recommended

accuracy value on average (± 0.5% specified by SHRP2) at a 95% confidence level. Results of the one-sided t-tests, shown in Table 4-7, indicate that the average deviation between mobile LiDAR point cloud, imagery-based point cloud, and field survey measurements was less than the minimum recommended accuracy value of ± 0.5% over the same length.

Table 4-7 Summary of Grade Deviations from Manual Survey Data

		Eastbound		Westbound	
		G_1 (%)	G_2 (%)	G_1 (%)	G_2 (%)
LiDAR	Min	0.01%	0.01%	0.0%	0.0%
	Max	0.16%	0.16%	0.11%	0.11%
	Mean	0.048%	0.046%	0.047%	0.04%
	Median	0.032%	0.03%	0.04%	0.03%
	One-sided t-test $H_a: \mu < 0.5$	t_{obs} -119.66	df = 99	P-value <0.0001	Significant Yes
UAV-CRP	Min	0.002%	0.02%	0.02%	0.01%
	Max	0.13%	0.13%	0.08%	0.08%
	Mean	0.046%	0.049%	0.058%	0.046%
	Median	0.03%	0.03%	0.07%	0.06%
	One-sided t-test $H_a: \mu < 0.5$	t_{obs} -56.49	df = 19	P-value <0.0001	Significant Yes

Comparison of Vertical Alignment and Sight Distance Data from Point Clouds

High-resolution surface models obtained from point clouds can be used to achieve realistic sight distance results (34). Point cloud data collected in this research were used to create 3D surface models representing the existing roadway surface using terrain modeling tools in OpenRoads Designer. As stated in the AASHTO green book, topography affects horizonal alignment, but it has an even bigger effect on vertical alignment. Vertical alignments were automatically created using extracted grade lines and best fit parabolas based on the road surface curvature obtained from the point cloud terrain models. Thus, a

semi-automated workflow was used to extract vertical alignment data along the centerline of the roadway in the eastbound and westbound travel directions.

Stopping sight distance is the distance required for a driver to perceive and react to an object in the roadway and come to a complete stop before a collision occurs (35, 36). Stopping sight distance may be computed using equation (4-5). Drivers must have a sight distance that is at least equivalent to the total stopping sight distance required at the design speed (37).

$$SSD = 1.47\,Vt + \frac{V^2}{30(F \pm 0.01G)} \qquad (4\text{-}5)$$

Where:

SSD = Stopping sight distance

V = Speed (mph)

t = Perception-reaction time (s) (2.5s assume based on AASHTO standards)

G = grade (%)

F = Coefficient of forward rolling or skidding friction.

A deterministic approach was used to compute sight distance on crest vertical curves using equation 4-6 and equation 4-7 based on an assumed eye height of 3.5 ft and an object height of 2.0 ft (AASHTO standards):

$$L = \frac{AS^2}{2158} \quad S<L \quad (4\text{-}6) \qquad\qquad L = 2S - \frac{2158}{A} \quad S>L \quad (4\text{-}7)$$

Where:

L = Length of vertical curve (ft)

S = Sight distance (ft)

A = Algebraic difference in grades (%)

Sight distance and design speeds estimated on crest vertical curves using manual survey and point cloud data are shown in table 4-8. Using Equation (4-5), design speeds were calculated based on sight distances obtained from extracted vertical alignment data.

Table 4-8 Vertical Alignment, Sight Distance, and Design Speed Estimates from Manual Survey and Point Cloud Data (Crest vertical curves).

Curve Type	Data	Travel Direction	VPC	VPT	Length	G1 %	G2 %	Sight Distance (ft)	Design Speed (mph)
Curve 2 (Crest)	Manual Survey	EB	184+74.66	199+35.91	1461.3	4.79%	-1.08%	733.25	74
	Vendor A	EB	184+82.19	199+40.94	1458.8	4.80%	-1.12%	728.97	73.8
	Vendor B	EB	184+82.39	199+56.01	1473.6	4.81%	-1.20%	727.41	73.7
	Vendor C	EB	184+78.86	199+64.01	1485.2	4.80%	-1.20%	730.86	73.9
	Vendor D	EB	184+79.64	199+62.94	1483.3	4.80%	-1.21%	729.80	73.8
	Vendor E	EB	184+77.49	199+64.76	1487.3	4.79%	-1.20%	731.99	73.9
	UAV-CRP	EB	184+73.59	199+63.88	1490.3	4.81%	-1.21%	730.91	73.9
	Manual Survey	WB	184+86.41	199+96.34	1509.9	4.83%	-0.81%	755.09	75.4
	Vendor A	WB	184+74.11	200+22.09	1547.9	4.89%	-0.91%	758.92	75.7
	Vendor B	WB	184+73.89	200+15.29	1541.4	4.89%	-0.89%	758.61	75.6
	Vendor C	WB	184+68.05	200+22.41	1554.4	4.90%	-0.90%	760.48	75.8
	Vendor D	WB	184+72.49	200+16.58	1544.1	4.89%	-0.89%	759.27	75.7
	Vendor E	WB	184+75.31	200+28.39	1553.1	4.87%	-0.92%	760.82	75.8
	UAV-CRP	WB	184+65.18	200+17.29	1552.1	4.90%	-0.89%	760.91	75.8
Curve 4 (Crest)	Manual Survey	EB	206+10.82	212+54.3	643.5	1.51%	-1.81%	647.62	66.3
	Vendor A	EB	205+73.63	212+70.97	697.3	1.66%	-1.84%	655.43	66.9
	Vendor B	EB	206+13.90	212+62.04	648.1	1.49%	-1.80%	652.03	66.6
	Vendor C	EB	206+16.94	212+78.13	661.2	1.47%	-1.85%	655.57	66.8
	Vendor D	EB	206+07.56	212+75.70	668.1	1.50%	-1.85%	656.05	66.9
	Vendor E	EB	206+14.89	212+76.87	661.9	1.48%	-1.86%	653.99	66.7
	UAV-CRP	EB	206+14.01	212+74.88	660.9	1.48%	-1.85%	654.43	66.7
	Manual Survey	WB	205+88.03	212+43.88	655.9	1.37%	-1.93%	654.79	66.7
	Vendor A	WB	205+97.29	212+36.41	639.1	1.39%	-1.93%	644.56	66
	Vendor B	WB	205+87.88	212+43.08	655.2	1.40%	-1.93%	651.61	66.5

	Vendor C	WB	205+91.86	212+46.25	654.4	1.39%	-1.94%	651.21	66.5
	Vendor D	WB	205+86.34	212+51.19	664.9	1.40%	-1.95%	654.44	66.7
	Vendor E	WB	205+82.85	212+53.33	670.5	1.42%	-1.97%	653.31	66.6
	UAV-CRP	WB	205+77.43	212+51.45	674	1.43%	-1.95%	656	66.8

Similarly, sight distance and design speeds estimated on sag vertical curves using manual survey and point cloud data are shown in Table 4-9. Equation 4-8 and equation 4-9 were used to calculate sight distance on sag vertical curves based on AASHTO standards:

$$L = \frac{AS^2}{400+3.5S} \qquad S<L \qquad (4\text{-}8)$$

$$L = 2S - \left(\frac{400+3.5S}{A}\right) \qquad S>L \qquad (4\text{-}9)$$

Where:

L = Length of vertical curve (ft)

S = Sight distance (ft)

A = Algebraic difference in grades (%)

Table 4-9 Vertical Alignment, Sight Distance, and Design Speed Estimates from Manual Survey and Point Cloud Data (Sag vertical curves).

Curve Type	Data	Travel Direction	VPC	VPT	Length	G1 %	G2 %	Headlight Distance (ft)	Design Speed (mph)
Curve 1 (Sag)	Manual Survey	**EB**	172+38.57	182+16.69	978.1	-2.33%	4.79%	576.40	59.2
	Vendor A	**EB**	172+31.55	182+19.91	988.4	-2.40%	4.80%	575.74	59.1
	Vendor B	**EB**	172+50.78	182+21.14	970.4	-2.31%	4.81%	572.27	58.9
	Vendor C	**EB**	172+47.89	182+21.14	973.2	-2.31%	4.80%	574.41	59
	Vendor D	**EB**	172+48.39	182+19.09	970.7	-2.31%	4.80%	573.13	58.9
	Vendor E	**EB**	172+49.02	182+17.82	968.8	-2.30%	4.79%	573.55	58.9
	UA CRP	**EB**	172+44.66	182+19.66	975	-2.33%	4.81%	573.23	58.9
	Manual Survey	**WB**	172+87.01	183+28.94	1042	-2.28%	4.83%	608.84	59.3
	Vendor A	**WB**	172+74.67	183+39.08	1064.4	-2.34%	4.89%	611.57	59.4
	Vendor B	**WB**	172+82.38	183+37.79	1055.4	-2.31%	4.89%	609.28	59.3
	Vendor C	**WB**	172+79.01	183+41.12	1062.1	-2.32%	4.90%	611.15	59.4

	Vendor D	**WB**	172+77.51	183+40.69	1063.2	-2.32%	4.89%	612.42	59.5
	Vendor E	**WB**	172+74.11	183+37.91	1063.8	-2.33%	4.87%	613.46	59.5
	UA CRP	**WB**	172+70.52	183+39.42	1068.9	-2.35%	4.90%	612.33	59.4
Curve 3 (Sag)	Manual Survey	**EB**	200+99.39	204+99.49	400.1	-1.08%	1.51%	858.06	76.4
	Vendor A	**EB**	201+01.09	205+26.95	425.9	-1.12%	1.66%	766.72	71.4
	Vendor B	**EB**	200+70.59	204+99.15	428.6	-1.20%	1.49%	825.96	74.6
	Vendor C	**EB**	200+75.62	204+93.21	417.6	-1.20%	1.47%	823.36	74.4
	Vendor D	**EB**	200+69.2	204+98.56	429.4	-1.21%	1.50%	814.35	73.9
	Vendor E	**EB**	200+72.42	204+95.44	423	-1.20%	1.48%	824.56	74.5
	UA CRP	**EB**	200+72.03	204+88.02	415.9	-1.21%	1.48%	807.99	73.6
	Manual Survey	**WB**	201+72.59	205+12.83	340.2	-0.81%	1.37%	1324.88	98.3
	Vendor A	**WB**	201+72.6	205+13.78	341.2	-0.91%	1.39%	1077.01	87.1
	Vendor B	**WB**	201+70.19	205+07.39	337.2	-0.89%	1.40%	1085.35	87.5
	Vendor C	**WB**	201+72.52	205+03.82	331.3	-0.90%	1.39%	1072.84	86.9
	Vendor D	**WB**	201+72.64	205+04.73	332.1	-0.89%	1.40%	1074.51	86.9
	Vendor E	**WB**	201+68.9	205+07.86	338.9	-0.92%	1.42%	1011.15	83.9
	UA CRP	**WB**	201+70.88	205+05.65	334.8	-0.89%	1.43%	1039.81	85.3
Curve 5 (Sag)	Manual Survey	**EB**	214+55.51	219+49.94	494.4	-1.81%	1.15%	772.21	71.1
	Vendor A	**EB**	214+55.88	219+36.81	480.9	-1.84%	1.11%	756.08	70.2
	Vendor B	**EB**	214+66.88	219+52.09	485.2	-1.80%	1.17%	754.54	70.1
	Vendor C	**EB**	214+51.54	219+58.46	506.9	-1.85%	1.18%	756.24	70.2
	Vendor D	**EB**	214+54.49	219+47.93	493.4	-1.85%	1.16%	748.10	69.7
	Vendor E	**EB**	214+48.68	219+57.09	508.4	-1.86%	1.18%	754.09	70.1
	UA CRP	**EB**	214+51.94	219+54.74	502.8	-1.85%	1.17%	755.30	70.1
	Manual Survey	**WB**	214+72.61	219+81.09	508.5	-1.93%	1.16%	735.16	69.6
	Vendor A	**WB**	214+69.99	219+82.26	512.3	-1.93%	1.16%	739.88	69.8
	Vendor B	**WB**	214+76.93	219+75.99	499.1	-1.93%	1.16%	724.66	68.9
	Vendor C	**WB**	214+79.78	219+67.88	488.1	-1.94%	1.14%	715.54	68.5
	Vendor D	**WB**	214+77.47	219+73.75	496.3	-1.95%	1.16%	714.50	68.4
	Vendor E	**WB**	214+71.75	219+65.84	494.1	-1.97%	1.14%	711.99	68.2
	UA CRP	**WB**	214+75.394	219+73.18	497.8	-1.95%	1.15%	719.67	68.7

To validate design speed data obtained from geometric features exacted from point clouds, a comparison was made with design speeds calculated using manual field survey data. Results of a paired t-test based on the means of speeds calculated from MLS data and speeds calculated from field survey data are shown in Table 4-10 and Table 4-11.

Table 4-10 Summary Statistics of Design Speeds Calculated Using Vertical Alignment Features Extracted from MLS Data (Eastbound).

EB Data	Curve 1 (Sag)	Curve 2 (Crest)	Curve 3 (sag)	Curve 4 (Crest)	Curve 5 (Sag)
Min	58.9	73.7	71.4	66.6	69.7
Max	59.1	73.9	74.6	66.9	70.2
Mean	59.0	73.8	73.8	66.8	70.1
Median	59.0	73.8	74.4	66.8	70.1
SD	0.06	0.10	1.36	0.13	0.19
	Paired t-test $H_a: \mu_d \neq 0$		t_{obs} =-1.34	P-value = 0.25 df = 4	

Table 4-11 Summary Statistics of Design Speeds Calculated Using Vertical Alignment Features Extracted from MLS Data (Westbound).

WB Data	Curve 1 (Sag)	Curve 2 (Crest)	Curve 3 (sag)	Curve 4 (Crest)	Curve 5 (Sag)
Min	59.3	75.6	83.9	66.0	68.2
Max	59.5	75.8	87.5	66.7	69.8
Mean	59.4	75.7	86.5	66.5	68.8
Median	59.4	75.7	87.0	66.5	68.4
SD	0.10	0.06	1.46	0.25	0.65
	Paired t-test $H_a: \mu_d \neq 0$		t_{obs} =-1.06	P-value = 0.35 df = 4	

These results indicate that there is a non-significant difference between the means of design speeds extracted from MLS point clouds and design speeds from manual survey data at a 95% confidence level. Thus, these results indicated that MLS data provide geometry features with enough accuracy to obtain reliable estimates of design speeds on crest and sag vertical curves of roadways.

Conclusions and Future Research

In recent years, several state transportation agencies have introduced programs to update highway feature inventories using emerging technologies such as MLS systems. Traditional data collection approaches can be costly, time-consuming, and less efficient. The objective of this study was to evaluate the accuracy of roadway geometry features including horizontal curve parameters, grades, and sight distance obtained using MLS and low-altitude UAV photogrammetry data for design speed estimation on horizontal and vertical curves of constructed roadways. MLS data were collected by LiDAR vendors who volunteered to participate in the study. Vendors were asked to provide the research team with adjusted and unadjusted data in the format requested. Participants who provided incomplete data were removed from the study. The study used MLS data collected by five vendors who provided data in the correct format. The results presented in this study are based on roadway geometry features extracted from adjusted point cloud data. Horizontal alignment comparisons indicated that the accuracy of geometry features extracted from MLS point clouds were within acceptable deviations recommended by SHRP2. Furthermore, results of statistical analyses indicate that MLS point clouds are a relatively more reliable source of accurate horizontal and vertical geometry data compared to UAV imagery-based point clouds based on acceptable deviations recommended by SHRP2. Results of statistical analysis on estimated design speeds on horizontal curves showed that the means of calculated design speeds from MLS and manual survey data are not statistically different at a 95% confidence level. Likewise, design speeds from UAV-imagery point clouds were similar to those obtained using manual survey data on average.

Lastly, the study showed that vertical alignment and sight distance estimates from MLS and UAV imagery-based point clouds were accurate enough to obtain reliable design speed estimates on vertical curves of constructed roadways based on statistical analysis results using a 95% confidence level. The effects of unadjusted point clouds on extracted horizontal and vertical alignment parameters for design speed estimation present an opportunity for future research.

REFERENCES

1. Yen, K. S., B. Ravani, and T. A. Lasky. LiDAR for Data Efficiency. Washington (State). Dept. of Transportation. Office of Research and Library …, 2011.

2. Federal Highway Administration (FHWA). Guide for Efficient Geospatial Data Acquisition Using LiDAR Surveying Technology. 2016.

3. Williams, K., M. J. Olsen, G. V. Roe, and C. Glennie. Synthesis of Transportation Applications of Mobile LIDAR. Remote Sensing, Vol. 5, No. 9, 2013, pp. 4652–4692. https://doi.org/10.3390/rs5094652.

4. Ogawa, T., and K. Takagi. Lane Recognition Using On-Vehicle Lidar. 2006 IEEE Intelligent Vehicles Symposium, 2006, pp. 540–545.

5. Kammel, S., and B. Pitzer. Lidar-Based Lane Marker Detection and Mapping. 2008.

6. Lindner, P., E. Richter, G. Wanielik, K. Takagi, and A. Isogai. Multi-Channel Lidar Processing for Lane Detection and Estimation. 2009.

7. Cheng, Y.-T., A. Patel, C. Wen, D. Bullock, and A. Habib. Intensity Thresholding and Deep Learning Based Lane Marking Extraction and Lane Width Estimation from Mobile Light Detection and Ranging (LiDAR) Point Clouds. REMOTE SENSING, Vol. 12, No. 9, 2020. https://doi.org/10.3390/rs12091379.

8. Yang, B., L. Fang, Q. Li, and J. Li. Automated Extraction of Road Markings from Mobile LiDAR Point Clouds. Photogrammetric Engineering & Remote Sensing, Vol. 78, No. 4, 2012, pp. 331–338.

9. Jung, J., E. Che, M. J. Olsen, and C. Parrish. Efficient and Robust Lane Marking Extraction from Mobile Lidar Point Clouds. ISPRS JOURNAL OF PHOTOGRAMMETRY AND REMOTE SENSING, Vol. 147, 2019, pp. 1–18. https://doi.org/10.1016/j.isprsjprs.2018.11.012.

10. Rastiveis, H., A. Shams, W. A. Sarasua, and J. Li. Automated Extraction of Lane Markings from Mobile LiDAR Point Clouds Based on Fuzzy Inference. ISPRS JOURNAL OF PHOTOGRAMMETRY AND REMOTE SENSING, Vol. 160, 2020, pp. 149–166. https://doi.org/10.1016/j.isprsjprs.2019.12.009.

11. Ravi, R., Y. T. Cheng, Y. C. Lin, Y. J. Lin, S. M. Hasheminasab, T. Zhou, J. E. Flatt, and A. Habib. Lane Width Estimation in Work Zones Using LiDAR-Based Mobile Mapping Systems. IEEE TRANSACTIONS ON INTELLIGENT TRANSPORTATION SYSTEMS, Vol. 21, No. 12, 2020, pp. 5189–5212. https://doi.org/10.1109/TITS.2019.2949762.

12. Che, E., M. J. Olsen, C. E. Parrish, and J. Jung. Pavement Marking Retroreflectivity Estimation and Evaluation Using Mobile Lidar Data.

PHOTOGRAMMETRIC ENGINEERING AND REMOTE SENSING, Vol. 85, No. 8, 2019, pp. 573–583. https://doi.org/10.14358/PERS.85.8.573.

13. Lin, Y., and J. Hyyppä. Geometry and Intensity Based Culvert Detection in Mobile Laser Scanning Point Clouds. Journal of Applied Remote Sensing, Vol. 4, No. 1, 2010, p. 43553.

14. Landa, J., and D. Prochazka. Automatic Road Inventory Using LiDAR. Procedia Economics and Finance, Vol. 12, 2014, pp. 363–370. https://doi.org/https://doi.org/10.1016/S2212-5671(14)00356-6.

15. Ural, S., J. Shan, M. A. Romero, and A. Tarko. ROAD AND ROADSIDE FEATURE EXTRACTION USING IMAGERY AND LIDAR DATA FOR TRANSPORTATION OPERATION. No. 2–3, Stilla, U and Heipke, C, ed., 2015, pp. 239–246.

16. Guan, H., J. Li, Y. Yu, C. Wang, M. Chapman, and B. Yang. Using Mobile Laser Scanning Data for Automated Extraction of Road Markings. ISPRS Journal of Photogrammetry and Remote Sensing, Vol. 87, 2014. https://doi.org/10.1016/j.isprsjprs.2013.11.005.

17. Gouda, M., B. A. D. Mello, and K. El-Basyouny. Automated Object Detection, Mapping, and Assessment of Roadside Clear Zones Using Lidar Data. TRANSPORTATION RESEARCH RECORD, Vol. 2675, No. 12, 2021, pp. 432–448. https://doi.org/10.1177/03611981211029934.

18. Findley, D. J., C. M. Cunningham, and J. E. Hummer. Comparison of Mobile and Manual Data Collection for Roadway Components. Transportation Research Part C: Emerging Technologies, Vol. 19, No. 3, 2011, pp. 521–540.

19. Gargoum, S. A., K. El-Basyouny, and J. Sabbagh. Assessing Stopping and Passing Sight Distance on Highways Using Mobile LiDAR Data. Journal of Computing in Civil Engineering, Vol. 32, No. 4, 2018. https://doi.org/10.1061/(asce)cp.1943-5487.0000753.

20. Gargoum, S., and K. El-Basyouny. Automated Extraction of Road Features Using LiDAR Data: A Review of LiDAR Applications in Transportation. 2017.

21. Ma, Y., Y. Zheng, J. Cheng, and S. Easa. Real-Time Visualization Method for Estimating 3D Highway Sight Distance Using LiDAR Data. JOURNAL OF TRANSPORTATION ENGINEERING PART A-SYSTEMS, Vol. 145, No. 4, 2019. https://doi.org/10.1061/JTEPBS.0000228.

22. Shalkamy, A., K. El-Basyouny, and H. Y. Xu. Voxel-Based Methodology for Automated 3D Sight Distance Assessment on Highways Using Mobile Light Detection and Ranging Data. TRANSPORTATION RESEARCH RECORD, Vol. 2674, No. 5, 2020, pp. 587–599. https://doi.org/10.1177/0361198120917376.

23. Agina, S., A. Shalkamy, M. Gouda, and K. El-Basyouny. Automated Assessment of Passing Sight Distance on Rural Highways Using Mobile LiDAR Data. TRANSPORTATION RESEARCH RECORD, Vol. 2675, No. 12, 2021, pp. 676–688. https://doi.org/10.1177/03611981211031235.

24. Cross, C., M. Farhadmanesh, and A. Rashidi. Assessing Close-Range Photogrammetry as an Alternative for LiDAR Technology at UDOT Divisions. Utah. Dept. of Transportation. Division of Research, 2020.

25. Bassani, M., N. Grasso, and M. Piras. 3D GIS BASED EVALUATION OF THE AVAILABLE SIGHT DISTANCE TO ASSESS SAFETY OF URBAN ROADS. International Archives of the Photogrammetry, Remote Sensing & Spatial Information Sciences, Vol. 40, 2015.

26. Farhadmanesh, M., C. Cross, A. H. Mashhadi, A. Rashidi, and J. Wempen. Highway Asset and Pavement Condition Management Using Mobile Photogrammetry. Transportation Research Record, 2021, p. 03611981211001855.

27. Nappo, N., O. Mavrouli, F. Nex, C. van Westen, R. Gambillara, and A. M. Michetti. Use of UAV-Based Photogrammetry Products for Semi-Automatic Detection and Classification of Asphalt Road Damage in Landslide-Affected Areas. ENGINEERING GEOLOGY, Vol. 294, 2021. https://doi.org/10.1016/j.enggeo.2021.106363.

28. Shams, A., W. A. Sarasua, A. Famili, W. J. Davis, J. H. Ogle, L. Cassule, and A. Mammadrahimli. Highway Cross-Slope Measurement Using Mobile LiDAR. Transportation Research Record, Vol. 2672, No. 39, 2018. https://doi.org/10.1177/0361198118756371.

29. South Carolina Department of Transportation (SCDOT). Roadway Design Manual. SCDOT, 2021.

30. Stein, W. J., and T. R. Neuman. Mitigation Strategies for Design Exceptions. United States. Federal Highway Administration. Office of Safety, 2007.

31. (AASHTO), A. A. of S. H. and T. O. A Policy on Geometric Design of Highways and Streets (7th Edition), Including 2019 Errata.

32. Zhang, K., and H. C. Frey. Road Grade Estimation for On-Road Vehicle Emissions Modeling Using Light Detection and Ranging Data. Journal of the Air & Waste Management Association, Vol. 56, No. 6, 2006, pp. 777–788.

33. Souleyrette, R., S. Hallmark, S. Pattnaik, M. O'Brien, and D. Veneziano. Grade and Cross Slope Estimation from LiDAR-Based Surface Models. 2003.

34. Castro, M., S. Lopez-Cuervo, M. Paréns-González, and C. de Santos-Berbel. LIDAR-Based Roadway and Roadside Modelling for Sight Distance Studies. Survey Review, Vol. 48, No. 350, 2016, pp. 309–315.

35. Robinson, B. W., L. Rodegerdts, W. Scarborough, W. Kittelson, R. Troutbeck, W. Brilon, L. Bondizio, K. Courage, M. Kyte, and J. Mason. Roundabouts: An Informational Guide. United States. Federal Highway Administration, 2000.

36. Rodegerdts, L. A. Roundabouts: An Informational Guide. Transportation Research Board, 2010.

37. Roess, R. P., E. Prassas, and W. R. McShane. Traffic Engineering 4th Edn.

CHAPTER FIVE

CONCLUSION

Advanced geospatial data collection technologies are becoming more readily available for various highway design, construction, and maintenance applications. These technologies include unmanned aerial systems (UAS), LiDAR systems, structure-from-motion, and close-range aerial photogrammetry. As shown in the studies included in this dissertation, benefits of these modern data collection technologies included enhanced efficiency, highly accurate and reliable data, and the ability to develop efficient and cost-effective data collection and processing workflows. The literature shows that state highway agencies continue to explore and introduce programs to update highway feature inventories using emerging technologies such as LiDAR systems. The primary goal behind such efforts is to improve the way in which roadway infrastructure systems are designed, built, and maintained. Another important benefit afforded by these technologies is the ability to identify and address constructability issues ahead of time using highly accurate three-dimensional data.

The primary objective of this research was to investigate if mobile LiDAR systems can be used as an effective means for collecting accurate system-wide data on existing roadways for various roadway safety evaluations. In addition, this research investigated whether close-range aerial photogrammetry could serve as a potentially inexpensive and effective alternative to LiDAR systems. The three studies included in this dissertation were designed and performed to help achieve the following four main objectives:

1. Evaluate if accurate cross-slope measurements can be extracted from point cloud-based 3D surface models and whether MLS and UAV-CRP data can be used for system-wide verification of highway cross slopes.
2. Compare curve design speeds estimated using horizontal alignment parameters extracted from point clouds, and whether MLS and UAV photogrammetry data can be used for system-wide verification of design speeds on horizontal curves.
3. Determine whether LiDAR and imagery-based point clouds can be used to estimate sight distance and design speeds on vertical curves.
4. In comparison with traditional surveying, investigate whether MLS and imagery-based point clouds can be used to produce accurate road surface models to estimate pavement material volumes for pavement resurfacing and rehabilitation purposes.

Paper I (Chapter 2) found that mobile LiDAR data could serve as an effective and reliable means for extracting cross slope data on existing roadways for system-wide verification (Objective 1). Additionally, the study showed that close-range aerial photogrammetry could potentially serve as a cost-effective alternative to LiDAR systems for collecting pavement surface information for cross slope verification. The use of mobile LiDAR and UAV imagery-based point clouds to extract cross slope measurements was evaluated on 10 test sections including 166 total measurements across four travel lanes in two directions along secondary road 1164, known as East West Parkway, located in

Anderson, SC. All data sets were calibrated using established control points for accurate comparison. Results of statistical analysis indicated that the achieved cross slope measurement accuracies were similar for measurements extracted from LiDAR and UAV-CRP data sets. The cross-slope data extracted from point clouds produced from LiDAR and UAV-CRP data met the minimum acceptable accuracy specified by SCDOT and SHPR2 of ±0.2%. Thus, the results of t-test statical analysis indicated that the average deviation between measurements extracted from point clouds and field survey measurements was less than the recommended acceptable accuracy of ±0.2% at a 95% confidence level. These findings help to identify existing roadway sections with inadequate cross slopes and enhance strategies to improve safety and minimize the potential for hydroplaning.

Paper II (Chapter 3) investigated the feasibility of using point clouds to obtain accurate road surface terrain models for pavement material volume estimation for resurfacing and rehabilitation purposes. The study focused on whether terrain models from MLS and UAV imagery-based point clouds could provide an effective and reliable means of estimating pavement material volumes in a cost-effective manner. Accurate methods for estimating material quantities are crucial in providing reliable estimates and minimizing costs. Terrain models from adjusted MLS data provided by five vendors, a terrain model from a UAV imagery-based point cloud, and a terrain model from manual survey data were compared based on calculated material volumes between surfaces using a surface-to-surface volume comparison method. The average difference in height between terrain models from MLS data ranged from 0.16 inches to 0.71 inches. The average difference

between terrain models from MLS and UAV imagery-based point clouds and a terrain model from field survey data ranged from 0.59 inches to 1.24 inches. This indicated that surfaces generated from either method could be used for material volume estimation purposes (Objective 4). However, the study found that using higher resolution UAV images and collecting additional ground control points could potentially improve the accuracy of pavement surface elevations. Thus, the use of surface models from point clouds to develop accurate material volume estimates would be highly beneficial to transportation agencies because the cost of traditional field surveying is typically higher than the overall cost of MLS and UAV photogrammetry surveys if used on a large scale. The proposed approach could make estimating pavement material quantities for resurfacing and rehabilitation more affordable for transportation agencies. However, the need for control surveys would not be eliminated since these surveys are important to enhance the positional accuracy of 3D point clouds.

Paper III (Chapter 4) evaluated the use of MLS and UAV imagery-based point clouds to estimate as-built horizontal and vertical geometry of roadways for design speed estimation on horizontal and vertical curves. The study found that point clouds from MLS and UAV photogrammetry data can be used to extract horizontal and vertical geometry data at sufficient accuracy to estimate design speeds on horizontal and vertical curves of constructed roadways (objective 2 and objective 3). The proposed approach offers advantages over extracting information from design drawings that may be unavailable, outdated, or inconsistent with the as-built roadway. Additionally, the proposed method can be used to identify locations where the posted speed limit/advisory speed is higher than the

design speed along horizontal curves so that corrective measures can be implemented on existing roadway networks. Identifying locations where vehicles may exceed design speeds is critical in preventing future crashes. Therefore, a proactive approach that identifies potential design deficiencies is favorable for analyzing crash data. Results were validated by analyzing deviations between geometry data and design speed calculations from point clouds and data calculated from manual field survey measurements using t-test statistical analysis at a 95% confidence level.

The use of remote sensing technologies such as MLS can improve data collection safety and efficiency by considerably reducing the time surveyors and other personnel are exposed to various safety risks associated with working in the field. As previously mentioned, studies have shown that automated surveying practices require less field time, enhance productivity, reduce crew sizes, and minimize human exposure. This research evaluated novel applications of MLS and UAV-CRP, further expanding on the many advantages of implementing MLS and UAV photogrammetry systems over conventional surveying techniques for certain applications.